

Hotspots and Mantle Plumes: Some Phenomenology

NORMAN H. SLEEP

Departments of Geology and Geophysics, Stanford University, Stanford, California

The available data, mainly topography, geoid, and heat flow, describing hotspots worldwide are examined to constrain the mechanisms for swell uplift and to obtain fluxes and excess temperatures of mantle plumes. Swell uplift is caused mainly by excess temperatures that move with the lithosphere plate and to a lesser extent hot asthenosphere near the hotspot. The volume, heat, and buoyancy fluxes of hotspots are computed from the cross-sectional areas of swells, the shapes of noses of swells, and, for on ridge hotspots, the amount of ascending material needed to supply the length of ridge axis which has abnormally high elevation and thick crust. The buoyancy fluxes range over a factor of 20 with Hawaii, 8.7 Mg s^{-1} , the largest. The buoyancy flux for Iceland is 1.4 Mg s^{-1} which is similar to the flux of Cape Verde. The excess temperature of both on-ridge and off-ridge hotspots is around the 200°C value inferred from petrology but is not tightly constrained by geophysical considerations. This observation, the similarity of the fluxes of on-ridge and off-ridge plumes, and the tendency for hotspots to cross the ridge indicate that similar plumes are likely to cause both types of hotspots. The buoyancy fluxes of 37 hotspots are estimated; the global buoyancy flux is 50 Mg s^{-1} , which is equivalent to a globally averaged surface heat flow of 4 mW m^{-2} from core sources and would cool the core at a rate of $50^\circ\text{C b.y.}^{-1}$. Based on a thermal model and the assumption that the likelihood of subduction is independent of age, most of the heat from hotspots is implaced in the lower lithosphere and later subducted.

INTRODUCTION

Linear seamount chains, such as the Hawaiian Islands, are frequently attributed to mantle plumes which ascend from deep in the Earth, perhaps the core-mantle boundary. The excessive volcanism of on-ridge hotspots, such as Iceland, is also often attributed to plumes. If on-ridge and midplate hotspots are really manifestations of the same phenomenon, one would expect that the temperature and flux of the upwelling material would be similar under both features. In particular, the core-mantle boundary is expected to be nearly isothermal so that the temperature of plumes ascending from the basal boundary layer should be the same globally provided that cooling by entrainment of nearby material and thermal conduction are minor. Finally, the global heat loss from plumes should imply a reasonable cooling rate of the core [Davies, 1988a].

The most important point of this paper is that the properties of mantle plumes are constrained by observations, mainly topography, geoid, and heat flow. I follow Davies [1988a], Richards *et al.* [1988], and Sleep [1987a, b] in assuming that the geometry of plumes consists of narrow vertical pipes which supplies hot mantle to a thin low-viscosity asthenosphere beneath the moving plate (Figure 1). Such plumes provide a much better explanation for geoid and topographic anomalies than does secondary convection from the cooling of the oceanic plate [Davies [1988a, b]. This geometry allows simplification of the discussion and the physics because the model plume is much narrower than the hotspot swell and the rapidly flowing layer of asthenosphere is thin compared to the thickness of the mantle and the width of the swell. The expense is some model dependency of the results primarily because the existence of a thin low-viscosity channel has not been established.

I begin by developing methods for estimating the flux of on-

ridge plumes using Iceland as an example. The geometry of flow implied by the assumed existence of a low viscosity asthenospheric channel is illustrated by this exercise. Then the methods for obtaining the flux of plumes on a rapidly moving plate are discussed with Hawaii as an example. These methods involve determining the flux from the plume from the cross-sectional area of the swell and taking advantage of the kinematics of the interaction of asthenospheric flow away from the plume and asthenospheric flow induced by the drag of the lithospheric plate. The methods for extending this approach to hotspots on slowly moving plates are then discussed with Cape Verde as an example. An estimate of the global mass and heat transfer by plumes is then obtained by applying the methods to 34 additional hotspots. The magnitude of this total estimated flux is compatible with the heat flux expected from cooling the core in agreement with Davies [1988a]. Finally, the results are used to obtain general properties of plumes and inferences on the underlying mantle dynamics.

ICELANDIC PLUME FLUX

The Icelandic hotspot is directly on the Mid-Atlantic Ridge. Methods developed for off-ridge hotspots are thus inappropriate. The excess volcanism of the ridge near the hotspot is probably the best way to constrain the excess temperature and volume of material supplied by the plume.

Excess Crustal Thickness and Temperature of Icelandic Plume

Higher temperatures beneath hotspot ridges lead to more partial melting and explain the 20-km-thick crust beneath Iceland [McKenzie, 1984]. An excess temperature of the upwelling material between 200°C and 250°C is needed to generate the excess 15 km of crust in the computations of McKenzie [1984]. This average excess temperature is also compatible with the depth and volume of extensive melting beneath Hawaii [McKenzie, 1984] and with the maximum excess temperature of 300°C of Wyllie [1988].

Copyright 1990 by the American Geophysical Union.

Paper number 89JB03587.
0148-0227/90/89JB-03587\$05.00

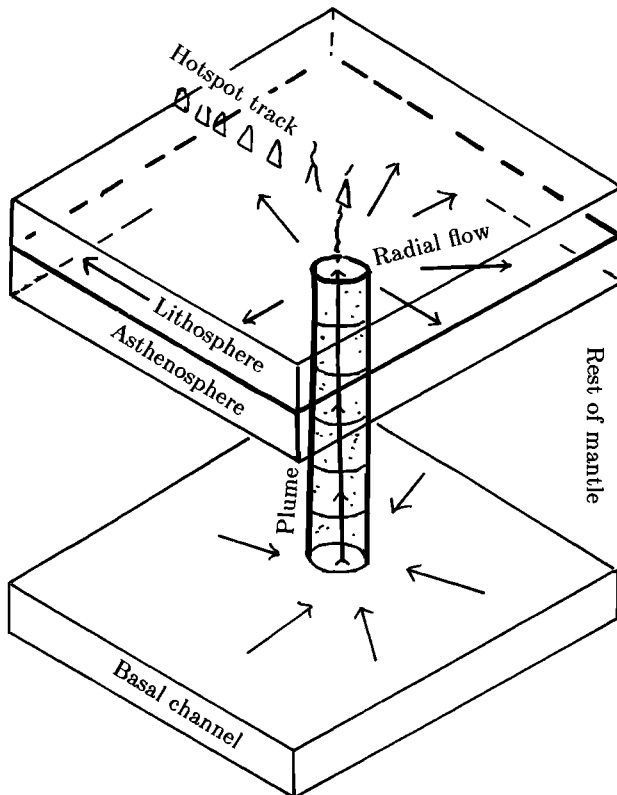


Fig. 1. Mantle plumes are envisioned to tap a basal channel near the core-mantle boundary and to discharge into the low-viscosity asthenosphere. The lithosphere moves over the plume creating a hotspot track. The radial flow in the asthenosphere away from the plume carries heat to the flanks of the swell.

Further quantification of these estimates would give more information on the temperature of the upwelling material. In addition, the geochemical anomaly provides information on the motion of the plume material [Schilling, 1986]. Unfortunately, the method of generation of mid-oceanic ridge basalts is not agreed upon. For example, Stolper [1980] and Elthon *et al.* [1982] state that mid-ocean ridge basalt (MORB) forms from a picritic melt generated around 70 km depth. In contrast, Presnall and Hoover [1984] state that extensive partial melting begins at 30 km depth. The former hypothesis implies that extensive melt remains in the mantle and thus precludes determining excess temperature from crustal thickness. Forms of the latter hypothesis are thus used by McKenzie [1984]. Fortunately, the various melting relationships used by McKenzie [1984] and a simplified relationship by Sleep and Windley [1982] give similar excess temperatures. I thus make no attempt to improve estimates of melting relationships. An estimate of 225°C for the average excess temperature of the Iceland plume is used below.

Flux of Icelandic Plume

The volume flux of the Icelandic plume may be computed from the kinematics of spreading. The plume needs to supply the oceanic lithosphere at least down to the depth of extensive melting, about 80 km, and probably the underlying asthenosphere as well. I assume that the plume flux balances the flow at a great distance (Figure 2). The flow is assumed to consist of a lithosphere moving at the plate velocity and an asthenosphere channel where the velocity decreases linearly from the plate

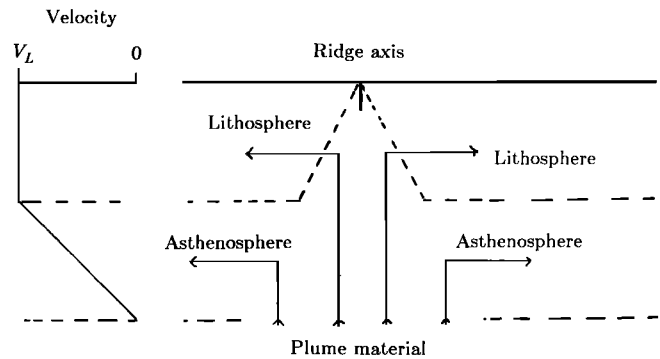


Fig. 2. The geometry of plate motion away from the Iceland hotspot is shown schematically. At large distances away from the hotspot, the flux of the plume is balanced by the flow in the lithosphere at the plate velocity V_L and the flow in the entrained asthenosphere. For convenience, both the lithosphere and the asthenosphere thickness are assumed to be 100 km in this paper.

velocity at the top to zero at the bottom. The volume flux is then

$$Q_p = V_S(L + A/2)Y \quad (1)$$

where V_S is the full spreading rate, L and A are the thicknesses of the lithosphere and the asthenosphere away from the ridge, here taken to be 100 km, and Y is the along-strike distance supplied by the plume.

Axial topography appears to correlate on a global basis with crustal thickness and magma chemistry variations attributed to higher temperatures in the ascending source material [Klein and Langmuir, 1987; 1989; cf. Brodholt and Batiza, 1989; Viereck *et al.*, 1989]. The distance supplied by the plume Y is therefore obtained from topography. An along-axis distance of 500 km of Iceland is supplied mainly by the plume, as it is either subaerial or shallow shelf. Several hundred additional kilometers where elevation and crustal thickness decrease away from Iceland are partly supplied by the plume. The geochemical anomaly extends over about 700 km [Schilling, 1986]. I obtain a flux of $63 \text{ m}^3 \text{ s}^{-1}$ by assuming an along-strike length of 800 km and a full spreading of 16.5 mm yr^{-1} [Gordon and Jurdy, 1986]. The volume flux of magma Q_v is $8 \text{ m}^3 \text{ s}^{-1}$.

It is useful to define a buoyancy flux for later comparison with off-ridge hotspots

$$B = \rho_m \alpha \Delta T Q_p \quad (2)$$

where ΔT is the average excess temperature, ρ_m is the density of the mantle, about 3300 kg m^{-3} , and α is the thermal expansion coefficient, about $3 \times 10^{-5} \text{ }^\circ\text{C}^{-1}$. The buoyancy flux of the Iceland plume is thus about 1.4 Mg s^{-1} . As shown below this flux is similar to the flux of Cape Verde and much less than the flux of Hawaii.

The Jan Mayen hotspot is supposed to exist along the ridge north of Iceland [e.g., Vink, 1984]. However, it has little topographic expression along the ridge axis. It is possibly related to southward propagation of the Moins ridge axis [Saemundsson, 1986]. The flux of this plume if it exists is included here in that of the Iceland hotspot.

HAWAIIAN PLUME FLUX

The Hawaiian hotspot is isolated from other features on the Pacific plate. Thus much speculation on mantle plumes and hotspots has used it as the primary example. The flux estimates

for the Hawaiian plume were obtained by *Davies* [1988a], *Richards et al.* [1988], and *Sleep* [1987a].

In this section, I discuss the origin of the topographic swell. Then, estimates of the flux of the plume and the average excess temperature of the plume material are obtained from kinematic considerations. Finally, the implications of geoid data are discussed.

Geometry and Origin of the Hawaiian Swell

The geometry envisioned for plumes in Figure 1 is convenient for discussion and the origin of the Hawaiian swell. Flow in the asthenosphere radiates out from the plume in all directions. Hot, less dense material occurs within the plume, within the asthenosphere, and within material moving with the lithospheric plate. Uplift of the seafloor occurs from the dynamic pressure gradient needed for material to flow in the asthenosphere away from the plume, more or less isostatic compensation of the material in the asthenosphere, and isostatic compensation of the material in the lithosphere. The first two effects are forms of dynamic compensation, which are considered separately as the asthenospheric channel is assumed to be thin compared to the depth from which plumes ascend.

In the case of Hawaii, these effects can be distinguished phenomenologically because the Pacific plate is moving rapidly (Figure 3). The uplift and geoid high from dynamic pressure

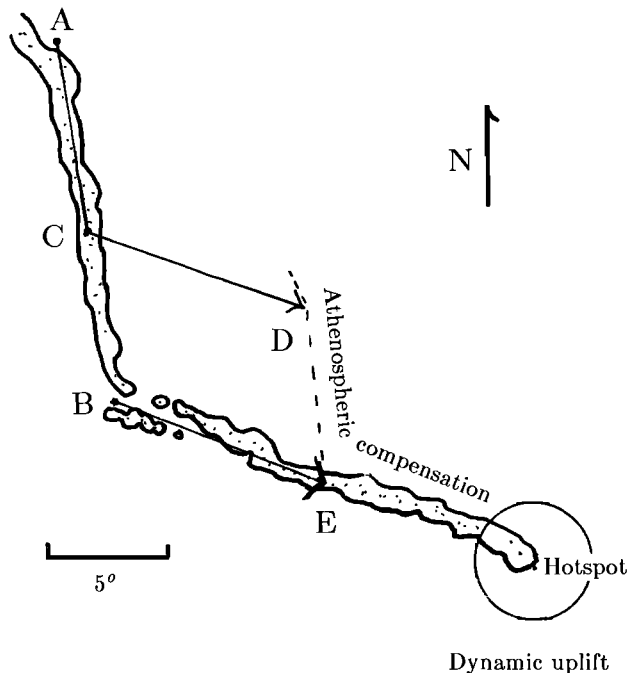


Fig. 3. The geometry of the Hawaii-Emperor chain permits distinguishing various causes of uplift and geoid highs. The volcanic chain after *Renkin and Sclater* [1988] is shaded. Hot lithospheric material moves with the plate and remains beneath the volcanoes. Asthenospheric material moves slower than the plate velocity. The path of material at a depth where the velocity is half the plate velocity is shown as an example. Hot asthenosphere discharged at the time that the hotspot was active at point A had moved to point C when the hotspot was active at the bend point B. This asthenospheric material is now at point D. The hot material implaced at B at the time of the bend has now moved to point E. Thus the Emperor chain and the western Hawaii chain are now underlain by normal asthenosphere rather than asthenosphere supplied by the plume. Dynamic uplift from radial flow from the plume is centered near the hotspot (500 km diameter circle).

should be centered on the plume. Excess elevation associated with excess lithospheric temperature moves at the plate velocity. Hot asthenospheric material moves at a velocity intermediate between the "fixed" velocity of the plume and the plate velocity.

The geometry of the Hawaii-Emperor bend is particularly revealing (Figure 3). As noted by *Crough* [1978] and *Detrick and Crough* [1978], the decrease in topography downstream (northwestward) along the chain and the subsidence of Midway Atoll are compatible with cooling of a heated lithospheric plate. The subsidence of a seamount in the Emperor chain would follow a similar thermal contraction curve if excess temperatures moved with the lithospheric plate. The situation is different, however, if a significant amount of the excess temperature resides in asthenosphere. Consider, for example, material at a middepth in the asthenosphere where the velocity is half the plate velocity. Such material is now in an L-shaped region defined by the younger half of the Hawaiian chain and a track parallel to the Emperor chain half the actual distance from the hotspot. At this depth, the older part of the Hawaiian chain and the Emperor chain are underlain by normal asthenosphere. In general, the hot asthenospheric material should have been swept eastward relative to the plate, such that the Emperor seamounts and the western part of the Hawaiian chain subsided more rapidly after the time of the bend, and the region east of the Emperor chain uplifted as hot material was swept under it.

Data from near the Hawaii-Emperor corner (or similar corners on other Pacific chains) are most useful as hot material had just been implaced into the asthenosphere at the time of the bend and small eastward displacements of hot material at the top of the asthenosphere relative to the lithosphere would cause the western side of the swell to subside more rapidly. Unfortunately, detailed subsidence data have not been obtained near the bend. The best approach is probably sedimentological studies of atolls and also, when available, turbidite flow directions on the deep sea. The Emperor chain and those parallel to it would be useful as they have not been underlain by asthenosphere from the plume since soon after the time of the bend. Current studies indicate the expected subsidence from cooling of rejuvenated lithosphere but lack resolution [*Schlanger et al.*, 1987]. In particular, the Midway subsidence record [*Detrick and Crough*, 1978] does not show any anomalous subsidence which could be attributed to normal asthenosphere being swept under the swell and replacing hot asthenosphere from the plume, but Pliocene and Pleistocene sea level changes make it difficult to examine the subsidence in detail.

The difference between crustal age and volcano age decreases northward along the Emperor chain [*Clague and Dalrymple*, 1987] making it difficult to recognize subtle variations in depth-age relationships or geoid. No excess elevation in the region east to the Emperor chain is evident on the maps of *Schroeder* [1984] and *Renkin and Sclater* [1988], and no geoid anomaly is evident on the maps of *Sandwell and Renkin* [1988]. However, the swell associated with the Emperor chain itself is not well resolved.

Early heat flow data [*Von Herzen et al.*, 1982] showed that the expected downstream increase as heat in the lower lithosphere is conducted to the surface and subsequent decrease as cooling occurs. Unfortunately, more recent data are scattered and do not demonstrate this trend [*Von Herzen et al.*, 1989].

In summary, *Detrick and Crough's* [1978] conclusion that the thermal anomaly is basically moving with the lithosphere is probably valid, but the actual distribution of excess heat in the asthenosphere is not yet well constrained.

Buoyancy Flux of Hawaiian Swell

The heat and mass budget of the Hawaiian swell is easily constrained because heat is carried away from the hotspot by the rapidly moving lithosphere at the same rate that it is supplied by the plume [Richards *et al.*, 1988; Davies, 1988a]. In particular, the cross-sectional area several hundred kilometers downstream from the hotspot, where the effects of less dense material in the asthenosphere and dynamic pressure are expected to be minor, has not been significantly reduced by cooling and thermal contraction. It is convenient to represent the mass anomaly associated with the swell by the buoyancy flux supplied to the swell by the plume:

$$B \equiv W \bar{E} (\rho_m - \rho_w) V_L = \overline{\Delta\rho_p} Q_p \quad (3)$$

where W is the width of the swell, \bar{E} is the excess elevation averaged across the swell, ρ_m is mantle density, ρ_w is water density, V_L is plate velocity in the hotspot frame, $\overline{\Delta\rho_p}$ is the average density reduction in the volume flux per time, and Q_p is volume flux of material supplied by the plume. For the Hawaiian swell the cross-sectional area $W \bar{E}$ is 1430 km^2 and the density contrast is about 2300 kg m^{-3} . I use a plate velocity of 83 mm yr^{-1} computed from Gordon and Jurdy [1986, Table 3]. Duncan and Clague [1985] obtain $86 \pm 2 \text{ mm yr}^{-1}$ from ages of volcanic rocks in the chain. The computed buoyancy flux is 8.7 Mg s^{-1} . (An extra decimal place is retained so that fluxes sum properly and can be compared.) Davies [1988a] gives a cross section of 900 km^2 and assumes a velocity of 96 mm yr^{-1} , implying a buoyancy flux of 6.3 Mg s^{-1} .

The buoyancy flux is readily related to heat flux from the plume. The mass reduction in a unit volume of the mantle is

$$\Delta\rho = \rho_m \alpha \Delta T \quad (4a)$$

where α is the thermal expansion coefficient (about $3 \times 10^{-5} \text{ }^\circ\text{C}^{-1}$) and ΔT is the excess temperature. The excess heat in this unit volume is

$$\Delta H = \rho_m C \Delta T \quad (4b)$$

where C is specific heat per mass (about $1.25 \times 10^3 \text{ J kg}^{-1} \text{ }^\circ\text{C}^{-1}$). The total excess heat flux, X , supplied by the plume is thus obtained from the ratio of $\Delta H/\Delta\rho$

$$X = B \frac{C}{\alpha} = \frac{C}{\alpha} \overline{\Delta\rho_p} Q_p \quad (5)$$

The excess buoyancy and the total excess heat flux are obtained directly from the cross-sectional area and plate velocity of the swell since the density, the heat capacity, and the thermal expansion coefficient of the mantle are well constrained.

Stagnation Point and Excess Temperature of Hawaiian Swell

The excess temperature in (2) of the average material supplied by the Hawaiian swell is more difficult to determine as the volume flux Q_p is unknown. Fortunately, the volume flux may be constrained kinematically from the shape of the nose of the swell. The basic point is that the flow in the asthenosphere away from the plume interacts with flow in the asthenosphere induced by the drag of the lithospheric plate. Quantification of this concept following Richards *et al.* [1988] and Sleep [1987a] introduces some model dependence into the numerical results. Material flows radially in the asthenosphere away from the plume permitting the model kinematics to be determined by conservation of mass (Figure 4). That is, the radial velocity of

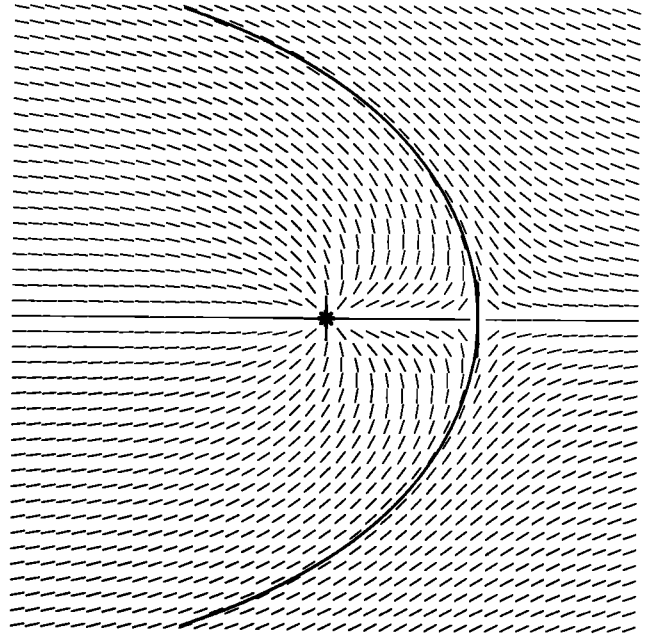


Fig. 4. Flow directions for the mean velocity of the asthenosphere are plotted with the plate moving to the left relative to the mantle. The stagnation streamline (dark line) separates asthenosphere on the left supplied by the plume (star) from normal asthenosphere on the right.

material in the asthenosphere decreases with the inverse distance from the plume

$$v_{\text{plume}} = \frac{v_f r_f}{r} \quad (6)$$

where the constant $v_f r_f$ is defined in terms of the reference velocity is v_f at the radial reference distance r_f . The average asthenospheric velocity when unperturbed by the plume is approximately half the plate velocity. A stagnation point thus occurs r_s upstream from the hotspot where the radial velocity from the plume is equal and opposite to the mean unperturbed velocity of the asthenosphere

$$\frac{v_L}{2} = \frac{v_f r_f}{r_s} \quad (7)$$

or solving

$$r_s = \frac{2v_f r_f}{v_L} \quad (8)$$

Normal asthenosphere exists outside the streamline defined by the stagnation point, while asthenosphere inside the stagnation point is supplied by the plume. Richards *et al.* [1988] and Sleep [1987a] have noted that the upstream end Hawaiian swell is shaped like a stagnation streamline, indicating that swell is reasonably explained by the presence of a plume. The stagnation distance r_s , obtained from topography of the Hawaiian swell is between 350 and 450 km.

The total flux of material from the plume is the material flowing outward at the reference distance r_f

$$Q_p = 2\pi r_f A v_f \quad (9)$$

where A is the thickness of the asthenospheric channel. Taking the reference distance to be the stagnation distance r_s where the reference velocity is $v_L/2$, the flux is

$$Q_p = \pi r_s A v_L \quad (10)$$

The average excess temperature from (2) is thus

$$\Delta T = \frac{B}{\pi r_s A v_L \rho_m \alpha} \quad (11)$$

Substituting for B from (3) yields

$$\Delta T \equiv \frac{W \bar{E} (\rho_m - \rho_w)}{\pi r_s A \rho_m \alpha} \quad (12)$$

which does not involve the plate velocity. The computed temperature depends inversely on the thickness of the asthenospheric channel which is the least constrained quantity in this equation. Assuming 100 km for this parameter, the 350-450 km range for the stagnation distance r_s yields average excess temperatures of 300°-230°C for the Hawaiian swell. The volume flux Q_p is about 300 m³ s⁻¹. In comparison, the flux Q_v of magmas implaced in the crust or erupted is about 4 m³ s⁻¹ [Watts and ten Brink, 1989]. The average fraction of plume material which melts Q_v/Q_p is about 1/10 that of Iceland. Most of the plume material beneath Hawaii remains at lower lithospheric depths where extensive melting does not occur, while plume material may ascend to shallow depths along the ridge axis and melt extensively beneath Iceland.

The fraction of heat carried to the surface by magma is

$$F_v = \frac{Q_v \rho_v C \Delta T_v}{Q_p \rho_m C \Delta T} \quad (13)$$

where the subscript v indicates the magma. Around 10% of the heat beneath Hawaii is extracted by magmas as the amount of cooling ΔT_v of the magma from its source temperature including the effects of latent heat is around 1800°C. Magma production is thus ignored in flux estimates for off-axis hotspots in this paper.

Geoidal Methods and Asthenospheric Flow

I have presumed that the plume is much narrower than the width of the Hawaiian swell and that downstream from the hotspot the excess temperature is moving basically with the lithosphere. A kinematic implication of these presumptions is that hot material flows laterally in the asthenosphere channel away from the plume and transfers its heat to the basal lithosphere by some small-scale convective process. That is, the asthenosphere is abnormally hot for a distance comparable to the width of the swell around the plume. Such hot asthenosphere provides an explanation for recent volcanism on the nose and flanks of the swell [Wallin, 1982; Lipman et al., 1989].

The hot material and the flow may be also detected by studying topography and geoid. That is, the lower density of the asthenospheric material tends to produce isostatic uplift. In addition, a pressure gradient is required for material to flow laterally in the lithospheric channel. These dynamic effects are conveniently treated separately as the asthenospheric channel is assumed to be thin. Neither effect is well resolved in the Hawaiian data.

Asthenospheric and lithospheric isostasy. The uplift from hot material in the lithosphere may be estimated by assuming perfect pointwise isostasy:

$$E_L = \frac{\rho_m}{\rho_m - \rho_w} \alpha \Delta T_L L \quad (14a)$$

where the factor involving densities adjusts for the effect of the water layer on isostasy and ΔT_L is the average excess temperature in the lithosphere of thickness L . Similarly, the uplift from hot asthenosphere is

$$E_A = \frac{\rho_m}{\rho_m - \rho_w} \alpha \Delta T_A A \quad (14b)$$

where ΔT_A is the average excess temperature in the asthenospheric channel of thickness A . The geoid anomaly is then the difference between the positive geoid anomaly for the excess topography and the negative geoid anomaly from the density deficiency at depth. This anomaly is approximately independent of wavelength [Turcotte and Schubert, 1982, p. 223].

$$\Delta N_A = \frac{2\pi G}{g_0} h_A E_A (\rho_m - \rho_w) \quad (15a)$$

where G is the gravitational constant, g_0 is the unperturbed surface gravity, and h_A is the average depth to the asthenospheric density anomaly, and similarly

$$\Delta N_L = \frac{2\pi G}{g_0} h_L E_L (\rho_m - \rho_w) \quad (15b)$$

where the subscript L indicates lithosphere. For example, 1.5 km of excess elevation compensated at 70 km depth implies a geoid anomaly of 10.3 m. Neglecting hydrodynamic effects for now, the observed elevation is the sum of elevation caused by the lithosphere and the asthenosphere

$$E_{\text{obs}} = E_L + E_A \quad (16)$$

The geoid height is similarly the sum of lithospheric and asthenospheric anomalies

$$N_{\text{obs}} = N_L + N_A \quad (17)$$

Substituting (15) into (17) would allow (16) and (17) to be solved for the two unknowns E_L and E_A .

The elevation anomaly and to a lesser extent the geoid anomaly are modified by lithospheric flexure and volcanic edifices. Some method is thus needed to estimate an uncontaminated elevation of the swell. Eyeball extrapolations [McNutt, 1984; Sleep, 1987a] give maximum excess elevations around 1.5 km for the Hawaiian swell. However, an inversion for the compensation depth, the maximum excess geoid height, and the excess elevation gave 70 km, 14 m, and 2.5 km, respectively [McNutt and Shure, 1986]. An inversion with an additional free parameter, the excess elevation produced by density anomalies in the asthenosphere, is unlikely to provide additional constraints without heat flow [see McNutt, 1987].

However, the magnitude of the expected effect of the swell being partly compensated in the asthenosphere is easily obtained from forward models. The main difficulty is that the magnitude and shape of the published measured geoid anomalies are strongly affected by filtering to remove long wavelength components (Figure 5). The computed model should be filtered in the same way as the published data. Fortunately, filtered anomalies may be computed directly by representing the excess masses of topography and the two compensating layers as a grid of point masses at the seafloor depth, the average lithospheric compensation depth, and the average asthenospheric compensation depth. Filtering schemes in common use are independent of the location of the pole or equivalently harmonics of all orders of the same degree are treated the same. A procedure is thus implemented by sequentially making each mass point the pole of the coordinate system. The filtered geoid anomaly then depends only on the distance between the mass point and the measurement point [Morse and Feshbach, 1953, p. 1274]

$$\Delta N = \frac{GM}{g_0} \sum_{n=2}^{\infty} f_n P_n(\cos \theta) \frac{r_0^n}{r_M^{n+1}} \quad (18)$$

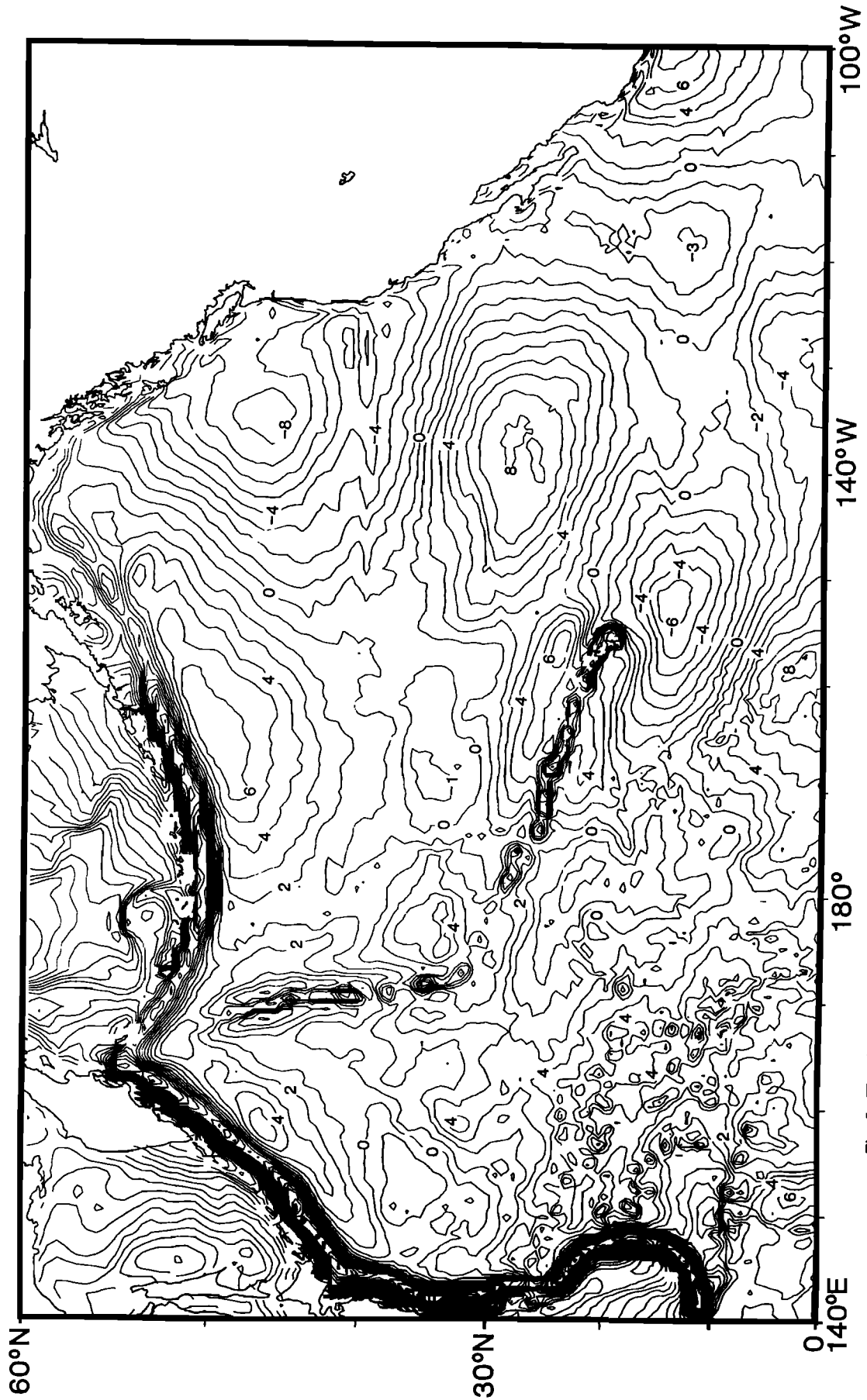


Fig. 5. The observed filtered geoid height (contour interval 2 m) was calculated by retaining spherical harmonic coefficients of degree 11 and above [Sanjwal and Renkin, 1988, Figure 2]. The geoid for the Hawaiian chain is significantly affected by flexural support of the volcanoes. Models predicting a 10-m high closed around the hotspot are not compatible with these data.

where θ is the angular distance between the measurement and the mass, G is the gravitational constant, g_0 is unperturbed surface gravity, M is the point mass, r_0 is the radius of the observation (and the Earth), r_M is the radius of the point mass, f_n are filter coefficients (which are all 1 for an unfiltered geoid), and n is the degree of the harmonic. The point mass for excess topography

$$M_{Ti} = E_{i,\text{model}} \Omega_i r_T^2 (\rho_m - \rho_w) \quad (19)$$

where $E_{i,\text{model}}$ is the modeled elevation at grid point i , Ω_i is the angular area represented by the grid point, and r_T is the radius excess topography. The point mass for lithospheric reduced density is

$$M_{Li} = -E_{i,L} \Omega_i r_L^2 (\rho_m - \rho_w) \quad (20)$$

where r_L is the average radius of reduced lithospheric density. Similarly, the point mass for asthenospheric reduced density is

$$M_{Ai} = -E_{i,A} \Omega_i r_A^2 (\rho_m - \rho_w) \quad (21)$$

where r_A is the average radius of reduced asthenospheric density and

$$E_{i,\text{model}} = E_{i,L} + E_{i,A} \quad (22)$$

for perfect isostasy. The complication that reduced density in the deeper parts of the asthenosphere may produce less surface topography than expected from perfect isostasy [Robinson *et al.*, 1987; Robinson and Parsons, 1988] is not included in the model as I am trying to show the difficulty in investigating even the simplest case. Permanent geoid and topographic anomalies associated with chemical differentiation [Robinson, 1988] are also ignored. Geoid height is calculated at each grid point by summing the geoid contributions at the relevant harmonic numbers for each point mass. The singularity from the point masses beneath the grid point itself is avoided by representing those three masses by disks with the same surface area as the grid elements.

A simple parameterization is used for the swell elevation and the compensating layers, as the objective is to examine the effect of compensation in the asthenosphere near the plume on geoid anomalies and the effects of filtering. The shape of the asthenospheric anomalous mass distribution is obtained partly from the kinematics of the assumed flow and conservation of energy [Sleep, 1987a]. The reader is referred to this paper for more detail.

The edge of the swell was defined by the stagnation streamline of Sleep [1987a] with the stagnation distance r_s taken to be 4° . Upstream of a distance $x > r_s$, the excess topography and the compensating layers are zero. In the distance range $-r_s \leq x \leq r_s$, the lithospheric anomaly is assumed to be

$$E_L = E_{\text{max}} \frac{(s-1)^2}{4} (1-t^2) \quad (23)$$

where E_{max} is the maximum elevation of the swell, here 1430 m. The normalized coordinate parallel to the axis of the swell is

$$s = x/r_s \quad (24)$$

where s is positive in the upstream direction. The normalized coordinate perpendicular to the axis is

$$t = y/y_s \quad (25)$$

where y_s is the distance from the axis to the stagnation curve at each point along the axis. The asthenospheric density anomaly is

$$E_A = E_{\text{max}} \frac{1-s^2}{2} (1-t^2) \quad (26)$$

This is equivalent to a 100-km thick layer with an excess temperature of 170°C in the asthenosphere beneath the hotspot. Downstream of $x = -r_s$, the asthenospheric compensating mass is assumed to be zero and the topography and the lithospheric mass are assumed to remain constant in width and to decay from cooling

$$E_L = E_{\text{max}} (1-t^2) \exp[-(x+r_s)/\lambda] \quad (27)$$

where t is normalized to the distance y_s at $x = -r_s$ and the decay distance λ is 100° . The s -dependent parts of the lithospheric and asthenospheric compensating anomalies are defined to conserve energy along the axial plane [Sleep, 1987a]. The t dependence is arbitrary but maintains continuity. The model topography and asthenospheric compensation are shown in Figure 6.

The excess topography, the lithospheric compensation, and the asthenospheric compensation were modeled as layers at 5, 75, and 155 km depth, respectively. The equator of the coordinate system was taken to be axis of the swell to maintain symmetry. The masses were represented on a 1° grid in latitude and longitude in this system. The swell was truncated 40° downstream from the hotspot, rather than attempting to model the Emperor swell. All harmonics above 101 were ignored; the upper limit in actual data is unclear. The effect of self-gravity in the filtered models is only a 2% increase and is ignored.

The effect of asthenospheric compensation as illustrated in Figure 7 is to increase the anomaly near the hotspot as expected. The increase is around 2 m and would not be easily resolved from the observed data. The effect of filtering is more complicated. The procedure of McNutt and Shure [1986] of retaining only the harmonics 11 and above results in side lobes as noted by those authors (Figures 7 and 8). The procedure of Sandwell and Renkin [1988] of using continuously varying filter coefficients to degree 25 ($f_n \equiv 1 - \exp(-(n-2)^2/16)$) gives only a small reduction of side lobes of the model (Figure 8). The unfiltered geoid is much larger than the filtered ones.

The large difference between the filtered and unfiltered geoids implies difficulties in previous approaches. Filtering cannot be dispensed with altogether because the low harmonics in the geoid are dominated by features unrelated to the swell. Residual geoid and topography may be obtained by removing effects associated with plate age and maybe slabs. There is some danger of making the same correction twice, once during filtering and once in making the residual [McNutt, 1988; Cazenave *et al.*, 1988]. In addition, the effects of the volcanic edifice and its compensation by the flexural moat around the seamount chain as well as the deeper compensation of the swell need to be considered. In practice, empirical methods are used to obtain "unfiltered" topography [Schroeder, 1984; McNutt, 1984] and geoid [McNutt and Shure, 1986] with the effects of flexure and the volcanic edifice removed. The amplitude, 14 m, and the closed high near the hotspot of around 2 m in the McNutt and Shure [1986] reduced geoid are compatible with the computed unfiltered geoid. Thus I conclude that abnormally hot material may exist in the asthenosphere beneath Hawaii, but it is not well resolved. The small amplitude, 2 m, of the predicted effect and the difficulties in obtaining a reduced observed geoid preclude an accurate estimate. Conversely, a very hot thick asthenosphere, for example, 100-km thickness and 1000°C excess temperature, would produce excessive uplift and geoid anomalies (10-m closure) and can thus be rejected.

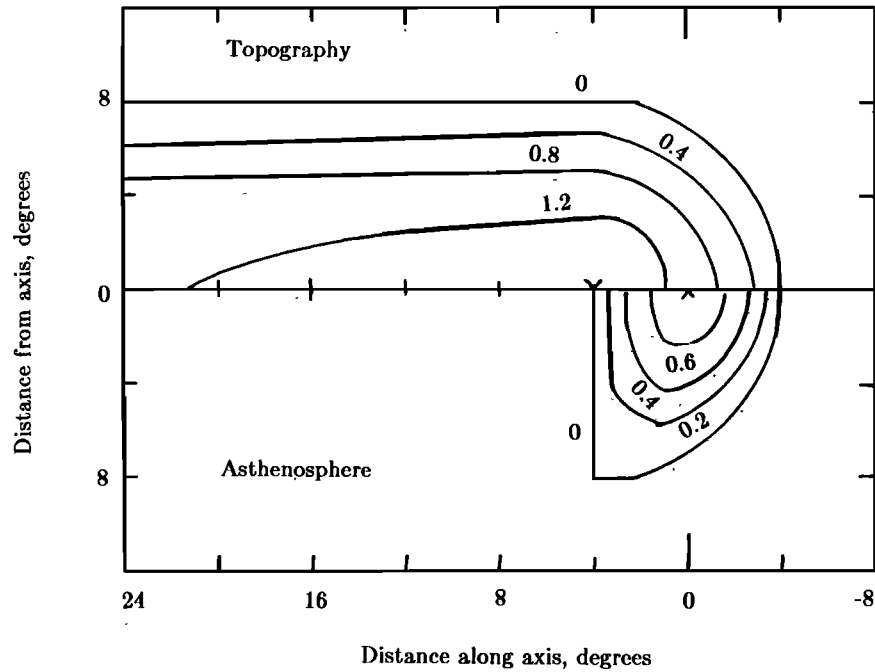


Fig. 6. The excess elevation of the parameterized Hawaiian swell is contoured in units of kilometers as a function of position on the swell (above). The maximum excess elevation of 1.43 km is indicated by a v. The uplift owing to asthenospheric compensation is contoured below. The maximum of 0.715 km is at the hotspot.

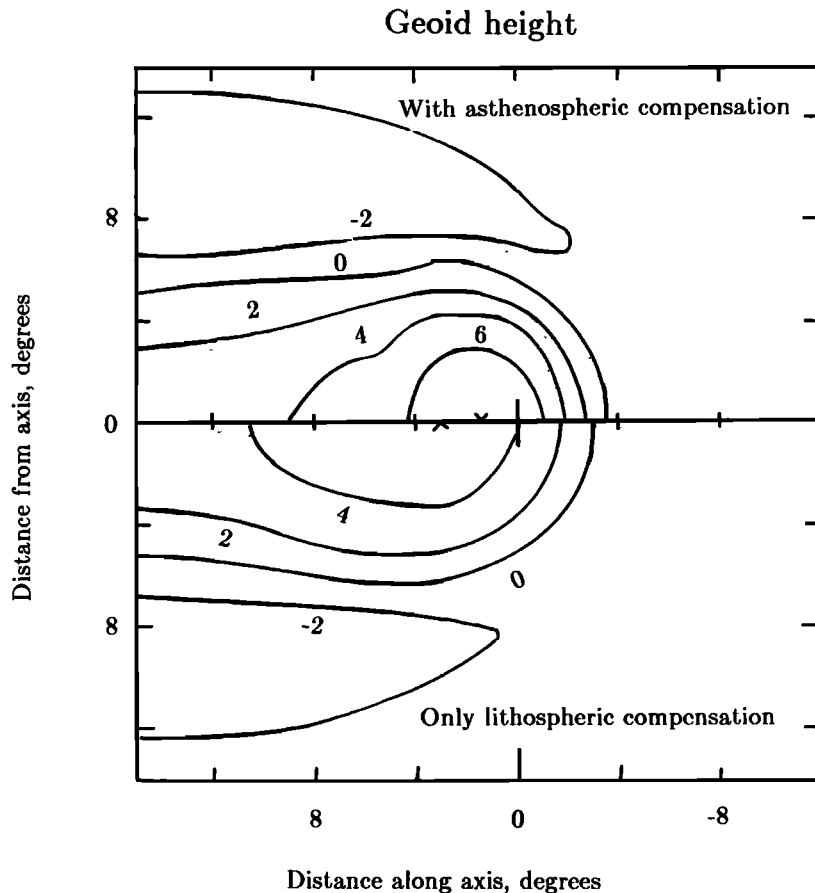


Fig. 7. The filtered geoid height in meters is shown for the model with asthenospheric compensation near the hotspot (above) and the model with only lithospheric compensation for the same uplift (below). The maxima are indicated with v's. Both models are filtered retaining degrees 11-101. The hotspot is at the origin.

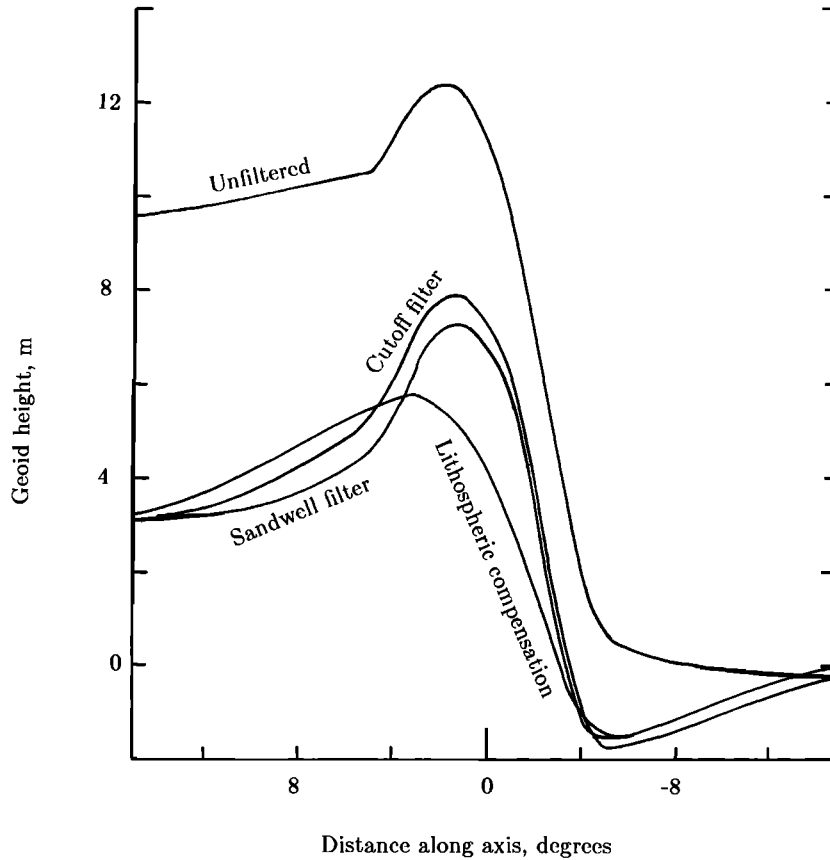


Fig. 8. The geoid height along the swell axis is shown for various models and filters. The hotspot is at the origin. The unfiltered model includes asthenospheric compensation. The model with the cutoff filter which retains degrees 11-101 is the first model in Figure 7. The smooth filter by *Sandwell and Renkin* [1988] reduces the side lobes a little. The second model in Figure 7 also uses the cutoff filter but has only lithospheric compensation. The computed geoid has no closed high near the hotspot.

Topography and geoid anomalies from dynamic pressure. The pressure gradient needed for asthenospheric material to flow outward from the plume is easily approximated by flow in a conduit between two parallel walls. The total radial volume flux (that is, the surface integral of horizontal velocity across an imaginary cylindrical surface a distance r from the axis of the plume) is approximately [Sleep, 1987b, equation (2)]

$$Q_A = \frac{-2\pi r}{12\eta_A} A^3 \frac{\partial P_A}{\partial r} \quad (28)$$

where η_A is the effective viscosity of the asthenospheric channel and P_A is the excess pressure in the asthenosphere. An uplift of approximately $P_A/(\rho_m - \rho_w)g$ is produced by the excess pressure.

The flux Q_A in (28) is approximately the plume flux Q_P in (10). However, the flux is not constant within a plume radius of the plume axis and also not constant at greater distances because material in the asthenosphere supplies a return flow to the deep mantle. These effects are represented in an analytical model by Sleep [1987b]. The plume is considered to be fed by a 100-km-thick, low-viscosity channel at the base of the mantle and discharge into a 100-km-thick, low-viscosity asthenosphere. For convenience, both channels were assumed to have the same viscosity. The mantle between the two channels has a constant higher viscosity. The model plume has constant radius, here 0.5° , and viscosity which was adjusted so that the buoyancy

flux is 10 Mg s^{-1} . The density reduction in the plume was assumed to be 30 kg m^{-3} .

The objective here is to obtain the shape of the geoid anomaly associated with dynamic flow in the asthenosphere rather than an estimate of asthenospheric viscosity which from (28) depends on the unknown quantity A^{-3} . Models were computed for intervening mantle viscosities of 10^{22} and 10^{21} Pa s and asthenospheric viscosities of 10^{19} - 10^{18} Pa s. Uplift and filtered geoid anomalies were computed (Figure 9). The computed geoid filtered to retain harmonics above degree 10 is mainly dependent on the flow in the asthenosphere and hence the quantity $\eta_A A^{-3}$. The intervening mantle viscosity affects the distance over which the radial flow occurs and the computed geoid at lower harmonics.

From Figure 9, it is evident that the computed topographic and geoid anomalies are strongest within 3° of the hotspot and thus may be obscured by the effects of isostatic compensation of the swell and flexural compensation of the volcanic edifice. The geoid anomaly and probably the excess topography are excessive for an asthenospheric viscosity of 10^{19} Pa s. That is, there is no 10-m closure in the observed geoid. The 3-4 m of geoid height for the models with an asthenospheric viscosity of 3×10^{18} are marginally acceptable. The less than 1-m heights for an asthenospheric viscosity of 10^{18} Pa s are acceptable in that they cannot be resolved in the data.

As most of the pressure gradient occurs within a few degrees

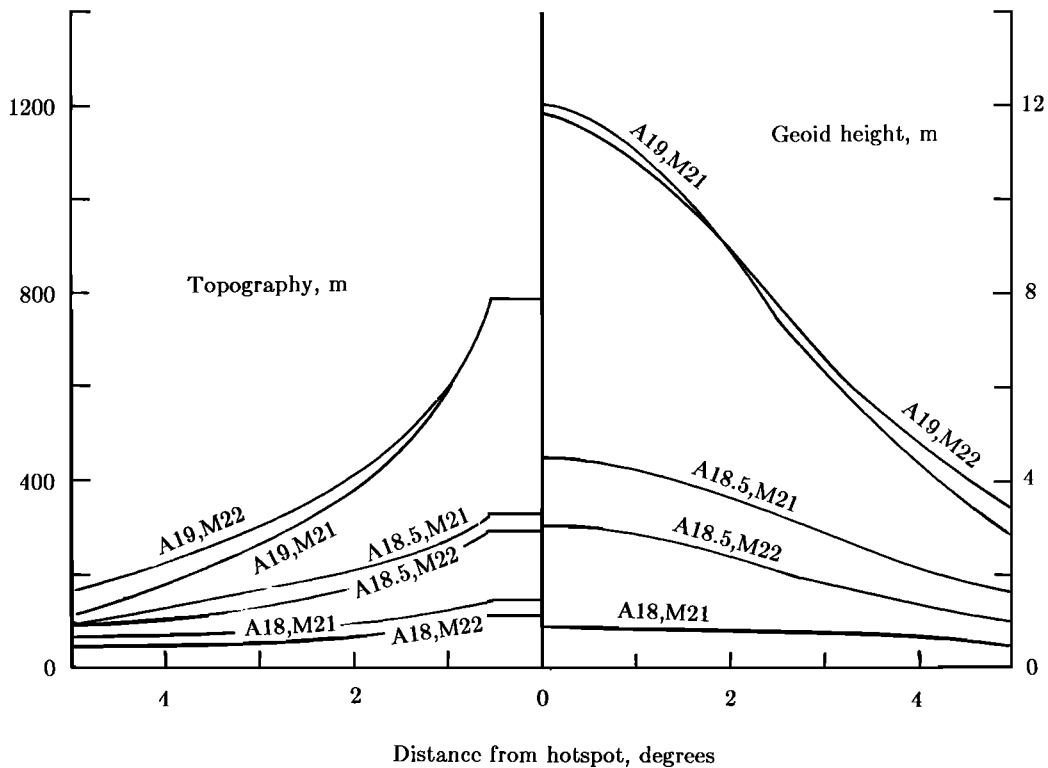


Fig. 9. The computed topography and geoid height for dynamic compensation near the swell are plotted as functions of radial distance from the axis of the plume. The model numbers indicate the logarithm of the asthenospheric (A) and the intervening mantle (M) viscosities in Pa s. The geoid anomalies are filtered retaining degrees 11-101. The models with high asthenospheric viscosity are unacceptable. The geoid height of model A18,M22 is too small to plot.

of the plume, the derived asthenospheric viscosity relates to asthenosphere partly charged with hot material from the plume. The distribution of viscosity around the plume should be laterally heterogeneous, but there is little point of more sophisticated models until a dynamic pressure effect is recognized. The upper limit of asthenospheric viscosity of about 3×10^{18} Pa s near the hotspot is compatible with the upper limits of asthenospheric viscosity near fracture zones of 10^{19} Pa s [Craig and McKenzie, 1986] and 10^{20} Pa s [Robinson et al., 1988]. However, the "normal" viscosity of Pacific asthenosphere is too poorly constrained to search for local variation near the hotspot.

It would be nice to conclude that dynamic pressure is also unimportant for all other hotspots, which, as shown below, have volume fluxes much less than Hawaii. The thickness and viscosity of the asthenospheric channel, however, may be different for each hotspot. Although I have found no example of significant dynamic pressure around a hotspot in the course of this work, examples of significant dynamic pressure around plumes may still be found. The reader is further cautioned that dynamic pressure and asthenospheric compensation can be separated only if a thin well-defined asthenospheric channel exists.

Average Excess Temperature of Hawaiian Plume

Crude estimates of the temperature of material in the asthenosphere beneath the Hawaiian hotspot and hence the average excess temperature of the Hawaiian swell were obtained above from the geometry of the stagnation point and from analyzing topography and geoid. The preferred estimate is around 200°C with considerable uncertainty, similar to the petrological esti-

mate of the average excess temperature of the Icelandic plume. This temperature needs to be compared with the maximum excess temperature at the center of the plume which provides evidence on the temperature contrast across the basal boundary layer. Fortunately, the volume flux and the temperature flux are easily computed in a tubular conduit [Sleep, 1987b]. For simplicity, it is assumed that viscosity varies as

$$\eta = \eta_M \exp(-\Delta T/T_\eta) \quad (29)$$

where η_M is the viscosity outside the plume is the normal mantle and T_η is a scaling parameter. The temperature difference at a point relative to the surrounding mantle is for convenience assumed to be the conduction solution [Carslaw and Jaeger, 1959, p. 258]

$$\Delta T = \Delta T_{\max} \exp(-r^2/r_p^2) \quad (30)$$

where ΔT_{\max} is the temperature contrast of the center of the plume which its surrounding and r_p is a measure of the radius of the plume. The flux of material through the plume is

$$Q_P \equiv \int_0^{r_I} 2\pi r v dr \quad (31)$$

where r_I is the upper limit of integration (here $2r_p$) and v is the vertical velocity within the plume assuming that flow is driven by the density contrast within the plume. That is, $v(r)$ is obtained by integration of the shear stress equation inward from r_I . The mean excess temperature of upwelling is

$$\bar{T} = Q_P^{-1} \int_0^{r_I} 2\pi r \Delta T v dr \quad (32)$$

The ratio $\bar{T}/\Delta T_{\max}$ depends of the total viscosity contrast across the plume or on $\Delta T_{\max}/T_{\eta}$. This ratio is 0.64 for 2 orders of magnitude viscosity contrast across the plume and 0.77 for 3 orders of magnitude. A 200°C average temperature contrast thus implies a maximum temperature contrast of 310°-260° C.

CAPE VERDE PLUME FLUX

The Cape Verde hotspot (Figure 10) is selected as an example of a plume on a slowly moving plate. Although uncertainties in the relative velocity of the hotspot to the underlying mantle create difficulties in the kinematic analysis of the swell, the slow velocity simplifies the analysis of heat flow and geoid anomalies.

Heat Flow and Asthenospheric Temperatures

Over 10 m.y. are required for heating of the lower lithosphere to produce a heat flow anomaly at the surface if only conduction is important. The heat flow anomaly for Hawaii is thus expected to be far downstream of the hotspot [Von Herzen *et al.*, 1982] and provides little evidence of the details of thermal structure at the hotspot. However, the Cape Verde hotspot has moved slowly relative to the lithosphere and a pronounced heat flow anomaly has had time to reach the surface [Courtney and White, 1986]. Volcanism and uplift began at least 20 m.y. ago in this area, long enough for heating in the deep lithosphere to produce the heat flow anomalies [McNutt, 1988; Courtney and White, 1986]. These authors conclude that at least part of the uplift and geoid anomalies are related to sublithospheric mass deficiency or dynamic uplift from fluid flow away from

the plume. Although Courtney and White [1986] and McNutt [1987, 1988] give detailed analyses, the essence of their reasoning is simply explained. Heating has been going on long enough that the geotherm from passive heating in the lithosphere without an underlying hot source (as would occur if the lower lithosphere delaminated and sank to great depth) should resemble the geotherm in younger oceanic crust. Thus the square-root-of-age law represents heat flow

$$q = q_0 \sqrt{t_a} \quad (33)$$

and topography

$$E = E_r - E_0 \sqrt{t_a} \quad (34)$$

where t_a is the apparent thermal age of the crust, the constant q_0 implies 500 mW m⁻² on 1-m.y.-old crust, the constant E_r is ridge elevation, and the constant E_0 implies subsidence of 350 m in the first million years. The heat flow anomaly relative to a half-space model is 20 mW m⁻² [Courtney and White, 1986] and the topographic anomaly is 1900 m [Courtney and White, 1986] to 2400 m [McNutt, 1988]. Taking the seafloor age as 125 Ma, the unperturbed heat flow is 45 mW m⁻². Heat flow 20 mW m⁻² higher is equivalent to 59 Ma crust. An elevation change of 1220 m is expected between normal crusts of these ages. Thus somewhere between 700 and 1200 m of the uplift may be attributed to sublithospheric effects. This is similar to the amount of thermal uplift in the asthenosphere obtained from the kinematic analysis of the Hawaiian swell.

The geoid anomaly is somewhere between 8 m [Courtney and White, 1986] and 12 m [McNutt, 1988]. These authors note that this anomaly is compatible with asthenospheric compensa-

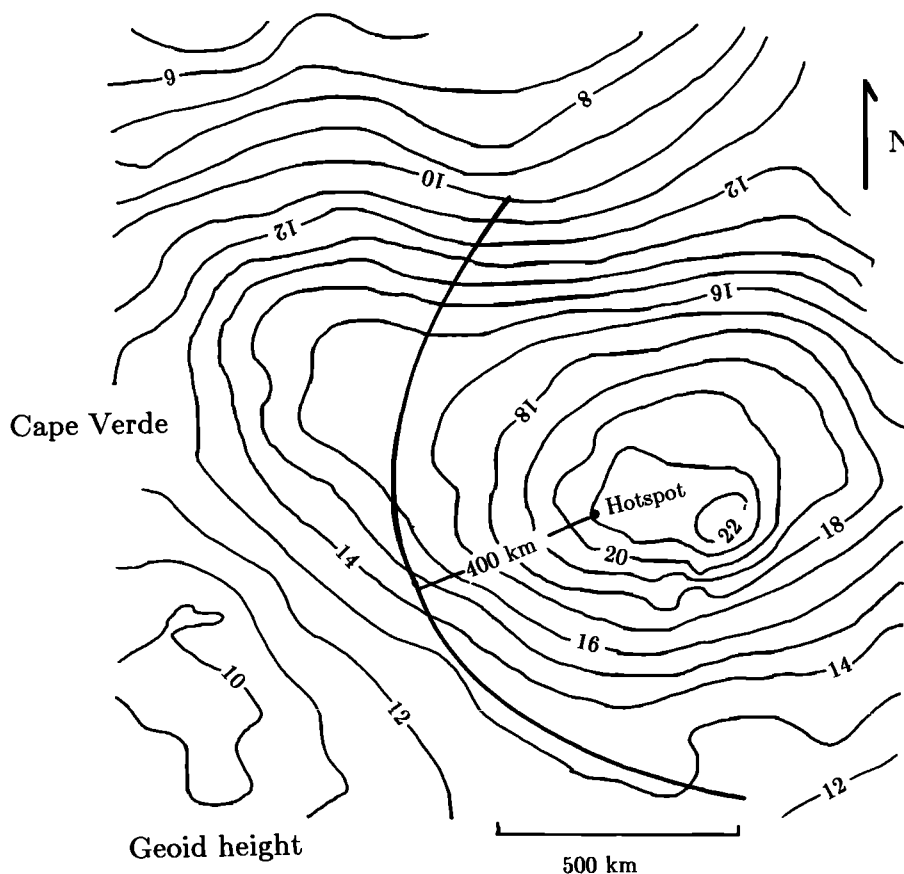


Fig. 10. The geoid height in meters [after Courtney and White, 1986] is contoured near the Cape Verde hotspot. The stagnation curve is fit by eye and is defined by the break in slope to the northeast and the 13-m contour to the southwest. The assumed position of the hotspot is indicated by a dot.

tion. As with Hawaii, the difficulties in filtering preclude obtaining more detail from the geoid anomaly.

Total Energy Flux and Volume Flux

The kinematic assumption that the plate is rapidly moving over a hotspot, which simplified analysis for Hawaii, is not appropriate for Cape Verde. An estimate of plume flux may be obtained from the shape of the swell. The global model used here [Gordon and Jurdy, 1986] predicts northeast to southwest movement of the hotspot relative to the lithosphere at 18 mm yr^{-1} . Unlike Hawaii, the absolute plate velocity is the source of considerable uncertainty for Cape Verde. For example, Courtney and White [1986] give 12 mm yr^{-1} and Duncan's [1984] tables imply 13 mm yr^{-1} . The tabulated direction and rate of the model hotspot are largely controlled by the Walvis Ridge to the south.

Unfortunately, the swell direction and the track direction are not clearly evident on either a geoid (Figure 10) or topographic map. If southwest propagation is assumed the geoid anomaly to the west northwest must be attributed to an unrelated feature, but the Cape Verde Plateau to the northeast is explained as the track. The swell front to the southwest may be fit to a stagnation curve (Figure 10). The stagnation distance of 390 km implies a volume flux of $70 \text{ m}^3 \text{ s}^{-1}$ for a plate velocity of 18 mm yr^{-1} (equation (10)). This is about about 1/4 of the Hawaiian flux.

The cross-sectional area of the swell after removing the 700 m of uplift for asthenospheric compensation obtained above by considering the geoid and heat flow is about 1200 km^2 , which implies a buoyancy flux of 1.6 Mg s^{-1} about 1/5 of the Hawaiian flux. Within the accuracy of the data, the average excess temperature, which is obtained from the ratio of buoyancy flux to volume flux, is the same for Hawaii and Cape Verde.

The hotspot has been stationary long enough that a minimum estimate of the total energy flux might be obtained from the surface heat flow. This requires extrapolating the data of Courtney and White [1986] over the area of the swell. From Figure 9 of Courtney and White [1986] the half width of the swell is 600 km and the average heat flow anomaly is about 10 mW m^{-2} . The length of the swell is 1500 km. This implies an excess heat flow of $1.8 \times 10^{10} \text{ W}$. Multiplying by α/C gives the equivalent buoyancy flux of 0.4 Mg s^{-1} which is much less than the direct estimate. The assumption that heat flow has come into steady state with heat supply is probably not justified. As discussed later, this is a general feature of hotspots, and much excess heat supplied to the lower lithosphere is ultimately subducted.

Cape Verde Results

In summary, the buoyancy and volume fluxes can be obtained for hotspots on slowly moving plates such as Cape Verde. One source of error is that the computed fluxes scale to the velocity of the plate which has a large relative uncertainty. Another is that material downstream from the hotspot has cooled significantly so that the cross-sectional area of the swell is determined right at the hotspot. A correction for uplift associated with hot material in the asthenosphere is thus needed. Fortunately, the correction is constrained by geoid and heat flow data.

The difficulty that lithospheric compensation alone can explain swells on the fast moving Pacific plate but that

asthenospheric compensation is needed on the slowly moving African plate [McNutt, 1988] may be an effect of sampling. For Hawaii, only a small fraction of the swell near the hotspot is underlain by abnormally hot asthenosphere, while the rest of the swell is compensated mainly in the lithosphere. Inversion for a single compensation depth will thus pick a lithospheric one appropriate for most of the swell. Conversely, hot asthenosphere underlies much of the Cape Verde swell and is more easily detected. Volcanic magmas also have more time to penetrate the lithosphere near Cape Verde and thus erupt away from the axis of the swell. In contrast, the flanks of the Hawaii swell are also underplated by hot material but volcanic activity, though present [Wallin, 1982; Lipman et al., 1989], is less obvious.

GLOBAL PLUME FLUX

The plume fluxes determined above vary by a factor of 6. A uniform average excess temperature of around 200°C is compatible with both geophysical and petrological data. I next apply the methods discussed above to 34 more plumes. Average plate velocities for the last 10 m.y. [Gordon and Jurdy, 1986] are used because material takes about that long to flow away from the plume to produce a swell. Consistent methods are used throughout so that the relative fluxes of plumes may be compared. Eyeball estimates for the cross-sectional area of swells and stagnation streamlines are used. The reader may easily adjust them if desired. The weakest hotspots have no obvious swells or geoid anomalies. The relative errors in their small fluxes are greater, and for the most part, upper limits are used as estimates.

For hotspots with swells, the method is similar to that of Davies [1988a]. The main differences are that Davies assumed that the cross-sectional areas of swells were all 750 km times the swell height and used plate velocities from Minster and Jordan [1978] and Pollack et al. [1981] which imply that the African plate is nearly fixed. Davies [1988a] used swell height, which is partly associated with thicker crust, to obtain an estimate for Iceland. He also made no correction for asthenospheric compensation. Although I obtain a similar global flux, more accurate estimates for individual plumes strengthen his conclusion and permit additional phenomenology.

Which Hotspots Are Associated With Plumes?

Not all off-ridge volcanism is necessarily associated with plumes. Some criteria to select hotspots are obtained from the phenomenological predictions of the plume theory. Mantle plumes, as envisioned here, supply hot material to the asthenosphere beneath hotspots. The hot material spreads laterally in the asthenospheric channel. Heat and material are exchanged between the lower lithosphere and the asthenosphere by convection. Even if plumes exist, some off-axis volcanism may be associated with cracks (see reviews by Sleep [1984] and Clague and Dalrymple [1987] for references).

The existence of well-defined hotspot tracks is evidence for plumes. In particular, Morgan [1981], Crough [1983], and Duncan [1984] have noted that several hotspot tracks have crossed a ridge axis either in the Atlantic Ocean or the Indian Ocean. If true, this is support for plumes originating at great depth. Cracks would be expected to stop when they reach a free edge. The evidence for anomalously hot asthenosphere and ascending material beneath Iceland, Hawaii, and Cape Verde is further strong support for plumes and against passive delamina-

tion along a crack. At present, the geophysical arguments that such hot material actually occurs are somewhat model dependent even for these hotspots. The other less studied and less isolated hotspots are ill suited for application of these methods. In principal, improved estimates of the amount of hot plume material in the source regions of on-axis hotspots could be obtained from petrological considerations following *Klein and Langmuir* [1987, 1989]. I do not attempt this here and use only topography.

Hotspots in regions of active rifting or recent continental breakup constitute a difficulty. *Morgan* [1981] shows that hotspot tracks weaken continental lithosphere so that breakup can occur. However, off-ridge volcanism is expected along the entire Atlantic margin before spreading becomes established. Postorogenic alkalic centers in Africa, Eurasia, and North America occur along preexisting weakness and thus are often attributed to intraplate stress [*Sykes*, 1978; *Black et al.*, 1985; *Giret and Lameyre*, 1985; *Bédard*, 1985; *McHone et al.*, 1987; *Stillman*, 1987]. For example, the Monteregean-Hills and White Mountain magma series in eastern North America, which is clearly associated with a seamount chain on the adjacent seafloor, is attributed by *Bédard* [1985] and *McHone et al.* [1987] to variations in intraplate stress. In addition, evidence on land from absolute ages of a well-defined track is equivocal [*McHone and Butler*, 1984]. Excessive volcanism along breakup margins is evidence for plumes [*White and McKenzie*, 1989]. However, *Mutter et al.* [1988] have proposed a delamination mechanism involving convection driven by the lateral temperature gradient along the breakup margin.

A further feature is that the hot material from plumes should spread laterally in the asthenosphere and be transported for large distances. Following *Schilling* [1973, 1986] and *Morgan* [1978], several areas of volcanism can be explained if plumes are considered sources of hot material that flows out rather than as separate point sources of heat. Some of the areas are easily explained in this way once one accepts the existence of plumes. The Reykjanes ridge is the result of hot material flowing away from the Iceland plume [*Schilling*, 1973, 1986] and Darwin Island is the result of material from the Galapagos plume reaching the spreading axis [*Morgan*, 1978]. Material entrained with the lithosphere is evidently the cause of Cocos Island northeast of the Galapagos hotspot [*Castillo et al.*, 1988]. Slowly moving plates loiter for a long time in the area of hot asthenosphere. For example, a single island in the Canary chain has a record of volcanism from 65 Ma to present [*Stillman*, 1987].

This late or prolonged volcanism also requires intraplate stresses favorable to the ascent of magma. Thus evidence of stress and structure control of volcanism does not preclude a plume source for the hot asthenosphere. In the compilation below, hotspots which have tracks in the general direction expected from plate motions are attributed to plumes. Some traditional hotspots are excluded: Jan Mayen is considered part of the Iceland hotspot as noted above. Madeira is included with Canary. The Comores Islands are considered to be a combination of a stress-related feature, near a continuation of the East African rift [*Grimison and Chen*, 1988], and hot material from older tracks. Amsterdam and Rodriguez are considered to be associated with hot material entrained into the ridge axis [*Morgan*, 1978]. Eifel is related to the Rheingraben. No attempt is made to separate stress- and plume-related features in Africa, except Hoggar, or to obtain fluxes for Mount Erebus and Raton. Only a preliminary estimate is obtained for Yellowstone. Revillagigedo near the intersection of the extinct Mathematicians spreading center [*Mammerickx et al.*, 1988] and

the active East Pacific Rise is considered to be stress related. Fortunately, as noted by *Davies* [1988a], these uncertain or omitted hotspots have small buoyancy fluxes.

Atlantic Hotspots

In addition to Cape Verde, *Duncan* [1984] lists the following hotspots in the Atlantic ocean south of 40°N: Azores, Madeira, Canary, Bermuda, Great Meteor, Fernando, Helena, Martin, Tristan, Discovery, Meteor, and Bouvet. The Bermuda hotspot is the most investigated geophysically. Hoggar is included in this section even though it is on the African continent. The Azores, Tristan, and Bouvet hotspots are modeled here as on-ridge features similar to Iceland.

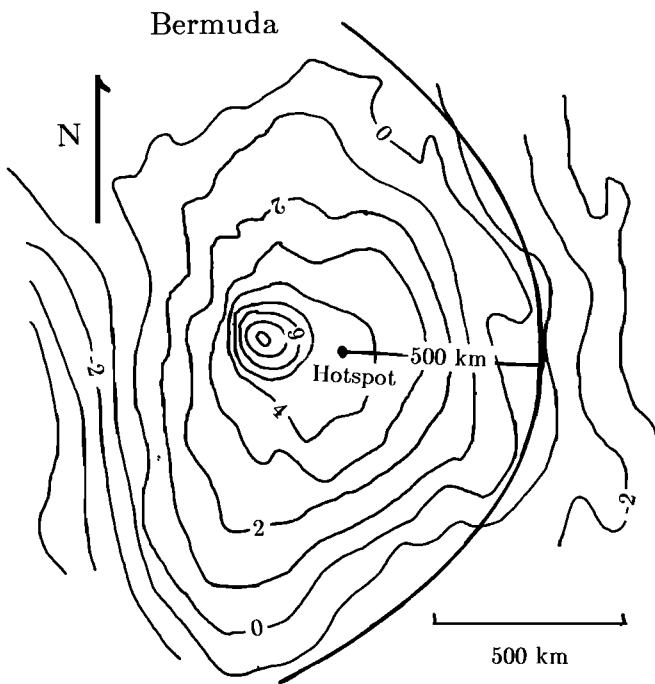
Bermuda. Bermuda is similar to Cape Verde in that it is on a slowly moving plate and that heat flow data are available. The hotspot is moving to the east. It also appears that activity has waned over the last 20-30 m.y. [*Detrick et al.*, 1986]. The present height of the swell is about 1000 m [*Crough*, 1983] and the wavelength is about 2000 km [*Detrick et al.*, 1986]. The heat flow is 57 mW m⁻² near the crest of the swell on 116 m.y. crust [*Detrick et al.*, 1986]. The expected half-space heat flow is 46 mW m⁻², and the apparent thermal age from the observed heat flow is 77 Ma. The expected elevation is thus 700 m. Thus about 300 m of uplift are associated with asthenospheric processes in general agreement with *Detrick et al.* [1986]. It is not unexpected that this is lower than the amount for Cape Verde because the Bermuda plume appears to have waned so that the hot asthenosphere supplied 40 m.y. ago has had time to cool. The computed flux is a measure of the average flux over that time and probably an overestimate of the current flux.

The cross-sectional area of the swell is about 1300 km². Making a correction for asthenospheric compensation yields a swell area of 1000 km². The plate velocity of 15 mm yr⁻¹ implies a buoyancy flux of 1.1 Mg s⁻¹. Assuming an excess temperature of 225°C gives a volume flux of 48 m³s⁻¹ and a stagnation distance of 320 km. The upstream part of the swell may be fit by a stagnation curve (Figure 11).

Other Atlantic off-ridge hotspots. Courtney, McNutt, Detrick, and their coworkers appear to have selected the hotspots with the strongest geoid anomalies for their studies. Bermuda and Cape Verde are both obvious in the filtered geoid maps of *Vogt et al.* [1984], *Bowin et al.* [1984], *Jung and Rabinowitz* [1986], and *Cazenave et al.* [1988]. No resolved anomaly is associated with Great Meteor, Fernando, Martin, Discovery, Meteor, and Helena. *Crough* [1983] gives swell heights of 1200, 500, 500, 600, 600, and 500 m, respectively. Obvious broad topographic swells are not associated with the latter four hotspots [*Hayes*, 1988, Figure 7].

A geoid anomaly is associated with the Canary hotspot, but it is somewhat obscured by the nearness to the African margin. This anomaly is most evident on the map of *Jung and Rabinowitz* [1986] and may be 2/3 of the Cape Verde anomaly. Madeira does not have a geoid anomaly independent of Canary and here is included in the Canary flux.

The fluxes from these plumes are thus not well constrained but cannot be large. I use a buoyancy flux of 1 Mg s⁻¹ for the Canary (including Madeira) hotspot and an upper limit flux of 0.5 Mg s⁻¹ for the other six hotspots. This history of the Great Meteor track will be discussed in detail in a future paper. The buoyancy flux when it crossed the ridge was less than 0.5 Mg s⁻¹; previously, it had been much stronger.



Geoid height

Fig. 11. The geoid height in meters near Bermuda is contoured in meters [Detrick *et al.*, 1986]. A 500-km stagnation curve is fit by eye to the anomaly. The model hotspot is at the dot. The single volcanic edifice is represented by the 6-m contour.

Other on-ridge Atlantic hotspots. The remaining on-ridge hotspots, Azores and Bouvet, have not produced large islands like Iceland. The temperature or the flux for these features is thus likely to be less than that of Iceland. In particular, the fluxes are likely to be too low to fully supply a length of ridge so that both plume material and normal mantle are entrained into the ridge axis.

The Bouvet hotspot is near a triple junction of ridges. The elevated crust associated with Bouvet Island extends about 100 km along the strike of the India-Antarctic ridge. Speiss ridge, which is on the next segment to the northwest extends over a similar distance [Sclater *et al.*, 1976, Plate 1]. The spreading rate on this segment is 16.6 mm yr^{-1} [Sclater *et al.*, 1976, Figure 6]. The buoyancy flux is thus about 1/4 of Iceland or 0.4 Mg s^{-1} .

Enhanced volcanism on the North American, Africa, and European plates is associated with the Azores hotspot. Subaerial volcanism occurs from Flores on the North American plate to Sao Miguel 500 km to the East on the Africa-Europe spreading center [Saemundsson, 1986]. However, a track is not obvious from the topography. The flux from this plume appears to be intermediate between Iceland and Bouvet. A large subaerial plateau has not formed but a 500-km-long region along the strike of the Mid-Atlantic Ridge is elevated and lacks a central rift. An elevated region is also produced along the third slowly spreading ridge. The spreading rate of the Mid-Atlantic Ridge here is somewhat more rapid (22 mm yr^{-1} to the south and 26 mm yr^{-1} to the north) than at Iceland, implying that more material is needed to supply the oceanic lithosphere at the ridge. Assuming that 450 km of lithosphere and asthenosphere come from the plume at a rate of 24 mm yr^{-1} , equation (1) gives a volume flux of $51 \text{ m}^3 \text{ s}^{-1}$ and a buoyancy flux of 1.1 Mg s^{-1} for this hotspot.

Tristan. The flux of the Tristan hotspot appears to have waned with time. In the Cretaceous Period, the Rio Grande Rise on the west and the Walvis ridge on the east were highly elevated platforms similar to Iceland at present. There were several ridge jumps before 71 Ma ago [Barker, 1983]. The flux at the time the Rio Grande ridge was active may be estimated by using the spreading rate of 52.6 mm yr^{-1} [Lawver *et al.*, 1985, Table 1] from 84 to 64 Ma and an effective ridge length of 800 km. This implies a volume flux of $200 \text{ m}^3 \text{ s}^{-1}$ and a buoyancy flux of 4.5 Mg s^{-1} .

The hotspot is now on the African plate and associated with a more subtle trace. The affected ridge length between Tristan and Gough is 800 km. The spreading rate from Gordon and Jurdy [1986] is 40.9 mm yr^{-1} . Assuming that the plume supplies half of the material over that length, the volume flux is $78 \text{ m}^3 \text{ s}^{-1}$, and the buoyancy flux is 1.7 Mg s^{-1} .

Hoggar. The Hoggar hotspot has been studied by Crough [1981]. The excess elevation is about 1 km. A track is not obvious from available data, but the edifice is aligned in the general direction of plate motion. Gordon and Jurdy's [1986] plate velocity is 20 mm yr^{-1} , and the cross-sectional area measured across the expected strike is about 400 km^2 . This implies a buoyancy flux of 0.9 Mg s^{-1} . (Note that a density contrast of 3300 kg m^{-3} is used for tracks on land.)

Tasman Seamount Chains

McDougall and Duncan [1988] define three hotspot tracks: one on the east coast of Australia, one in the center of the Tasman basin, and one on the east of the Tasman basin. Propagation to the south is demonstrated by absolute ages of volcanic rocks from the first two seamount chains. The expected propagation rate from Gordon and Jurdy [1986], 63 mm yr^{-1} , agrees with this progression. Two of the chains occur along conjugate rift margins, and the third occurs along the extinct spreading center of the Tasman basin. Without the excellent evidence for tracks, this volcanism would probably be attributed to intraplate stress.

The widths of the swells associated with the two marine tracks are not evident. The seamounts have subsided similarly to the rate expected if they rest on normal oceanic crust. For example, Recorder seamount which rests on 55 Ma crust has subsided 500 m since 25 Ma [McDougall and Duncan, 1988]. The expected subsidence is 680 m. Even allowing time for the seamount to erode and for reduced apparent subsidence from sealevel decrease, only a few hundred meters of extra subsidence are permitted by the data. For example, subsidence of 900 m over the last 25 m.y. would imply resetting of the apparent age to 23.5 Ma from 30 Ma and an uplift of 200 m.

The width of uplift of the track along the coast of Australia may be determined from topography and the scatter of volcanic centers from the track. Uplift is harder to determine as the track follows a young Atlantic type margin. If 700 m of uplift and 300 km cross section are assumed, then the cross-sectional area is 140 km^2 . The buoyancy flux is 0.9 Mg s^{-1} . The two marine tracks appear to have waned and have sparse volcanism at present. The flux of the land hotspot is an upper limit for the other two tracks. The current flux could be much smaller.

Pacific Hotspots

Numerous active hotspots in addition to Hawaii occur in the Pacific basin. Unfortunately, it is more difficult to estimate the fluxes of these hotspots than it is for Hawaii. The southern

Pacific hotspots are closely spaced and sometimes considered a hot line [Bonatti *et al.*, 1977]. The near-ridge hotspots, Cobb on the Juan de Fuca ridge, Easter on the East Pacific Rise, and the Galapagos hotspot have not created large areas of subaerial ridge like Iceland.

Superswell hotspots. McNutt and Fischer [1987] have called the topographic feature associated with the Easter, Pitcairn, Marquesas, Macdonald, and Tahiti hotspots the Pacific Superswell. This feature is not simply overlapping swells. Hot material is entrained at the ridge and the depth-age relationships are different from normal crust. It is hard to determine the flux of individual plumes because hot material vented into already hot asthenosphere produces no additional anomaly. The total buoyancy flux of 13.3 Mg s^{-1} can be estimated from the cross sectional area of 2200 km^2 in Figure 3 of McNutt and Fischer [1987] and the plate velocity of 83 mm yr^{-1} . Davies [1988a] gives a total buoyancy flux of 15.9 Mg s^{-1} . Attributing this flux to the four off-ridge hotspots gives a buoyancy flux of 3.3 Mg s^{-1} to each, about 3/8 of Hawaii. The stagnation distance for this flux is less than 200 km precluding swells which can be easily distinguished from the effects of flexure and the volcanic edifice. Heating of the lithosphere is recognized mainly through the subsequent subsidence of atolls [e.g., Detrick and Crough, 1978]. The situation is thus analogous to the older Marshall island track where multiple heating events and eventual cooling are indicated by studies of sediments [Schlanger *et al.*, 1987].

The Caroline, Samoa, Juan Fernandez, and San Felix hotspots are probably weaker than the other South Pacific hotspots. Crough [1983] gives no swell heights for the former two hotspots and heights of 500 and 700 m for the latter. None of them have obvious swells. The Caroline hotspot appears to have weakened as the volcanic edifices decrease to the east [Keating *et al.*, 1984]. Samoa is near the Tonga arc. Some more recent volcanism may be associated with flexure [Wright and White, 1987]. Juan Fernandez and San Felix have been attributed to intraplate stress similar to that which broke the plate along the Galapagos spreading center [Mammerickx, 1981]. There is some possibility that San Felix taps hot material entrained by the plate at the Easter hotspot. Half of the flux of the other superswell hotspots is assigned to these four hotspots.

Louisville. The Louisville hotspot has waned drastically [Watts *et al.*, 1988; Lonsdale, 1988]. It is marked now only by a small volcano at 138.1°W . The seafloor is at most 300 m shallower than the expected 4800 m depth of 43 Ma crust. Bathymetry and geoid data are insufficient to define the active end of the swell. The flux of this hotspot is clearly less than the smaller superswell hotspots. I assign as an upper limit the flux of 0.9 Mg s^{-1} as the hotspot and plate velocity are similar to the Tasman Sea chains. As will be discussed in a future paper, it was previously much stronger.

Pacific near-ridge hotspots. The flux of the Easter hotspot may also be estimated from the along-strike area where the ridge crest is elevated. Unlike Iceland and to some extent the Azores, a large area of subaerial exposure is not produced. The main effects of this hotspot extend about 300 km along strike. Part of the flux of the plume is returned to the East Pacific Rise, part remains on the Nazca plate, and a little crosses the ridge and ends up beneath either the Easter microplate or the Pacific plate. I assume that half the lithosphere and the asthenosphere of the spreading ridge along an equivalent length of 300 km is related to the plume and that the full spreading rate is

200 mm yr^{-1} . The volume flux is thus $140 \text{ m}^3 \text{ s}^{-1}$. Assuming an average temperature of 225°C the buoyancy flux is 3.3 Mg s^{-1} , equivalent to the average for the superswell hotspots.

The Galapagos hotspot is strong enough to produce seamount chains on each side of the spreading center and also to be associated with various ridge reorganizations [Hey, 1977; Hey *et al.*, 1977]. The strongly affected region is again about 300 km long, but the full spreading rate is only 60 mm yr^{-1} . Thus the volume flux is $43 \text{ m}^3 \text{ s}^{-1}$, and the buoyancy flux is 1.0 Mg s^{-1} .

Northeast Pacific hotspots. The Juan de Fuca and Bowie hotspots are associated with ill defined chains. Neither feature shows any anomalous Sr isotope ratios [Eaby *et al.*, 1984; Allan *et al.*, 1988]. It is possible that both chains are not associated with plumes but are stress-related effects of reorganization of the ridge axis and nearby plate boundaries. Flow of material from the Yellowstone plume or the plume head associated with the Columbia basalts is another possibility. The approach of the Juan de Fuca hotspot toward the ridge as expected from absolute velocities is the strongest evidence for considering it to be a plume [Karsten and Delaney, 1989]. These hotspots are discussed to show that the fluxes of their plumes, if they exist, are small.

The Juan de Fuca hotspot is clearly much weaker than the Galapagos one. No islands are produced and the hotspot does not produce large seamounts on both sides of the axis. The region with excess elevation is only 100 km long. Assuming that the plume supplies half the material over that length gives a volume flux estimate of $17 \text{ m}^3 \text{ s}^{-1}$ and a buoyancy flux of 0.3 Mg s^{-1} .

This estimate is also used for the nearby Bowie seamount chain for which Crough [1983] gives a swell height of 300 m. A well-defined track is not associated with Bowie [Dalrymple *et al.*, 1987]. It is unclear whether this hotspot is on-ridge at Dellwood Knolls or off-ridge near Bowie. Following Duncan and Clague [1985], I consider Bowie hotspot to be on the ridge. The same flux estimate is also assigned to the Baja hotspot which is associated with a similar ill-defined chain.

Yellowstone. The Snake River plain defines the track of the Yellowstone hotspot. The propagation rate, 35 mm yr^{-1} is defined by a variety of studies [Anders *et al.*, 1989]. The thermal uplift is about 1 km from the subsequent subsidence and from heat flow data [Brott *et al.*, 1981]. The cross-sectional area for the swell and the distance to the stagnation point are much more difficult to determine as uplift needs to be separated from previous elevation differences. More field work is needed to relate seismicity and field geology to uplift ahead of and lateral to the hotspot track (M. Anders, personal communication, December 1988). It is important to determine if this continental feature is similar to oceanic hotspots. For now, the cross-sectional area of the swell is assumed to be 400 km^2 , giving a buoyancy flux of 1.5 Mg s^{-1} .

Indian Ocean Hotspots

The Crozet, Réunion, and Kerguelen hotspots have produced tracks in the Indian Ocean [Morgan, 1981]. The Afar hotspot has produced a subaerial plateau near a triple junction.

Crozet. Crozet is similar to Cape Verde in that the excess heat flow, the excess topography, and the geoid anomaly imply some compensation in the asthenosphere [Courtney and Recq, 1986]. The hotspot is placed by Morgan [1981] beneath the Del Cano plateau near 45°S , 45°E . However, the Del Cano

feature appears to be much more shallowly compensated than the Crozet Bank to the east [Goslin and Diament, 1987; Sandwell and MacKenzie, 1989]. I place the hotspot near the Crozet Islands around 46°S , 50°E (Figure 12). A stagnation curve with $r_s = 140\text{ km}$ may be fit to the west-northwest end of the swell. The expected plate motion, however, is $\text{N}96^{\circ}\text{W}$. A volume flux of $22\text{ m}^3\text{ s}^{-1}$ is obtained from the stagnation distance of 140 km and a plate velocity of 16 mm yr^{-1} . Again assuming an average excess temperature of 225°C , the buoyancy flux is 0.5 Mg s^{-1} , similar to what I have assigned to other weak hotspots.

Kerguelen. The Kerguelen track has crossed the ridge axis. The current elevation anomaly is difficult to separate from the plateau formed while the hotspot was closer to the ridge [Storey et al., 1989]. The history of this track is thus too complicated to resolve here and the Crozet flux assigned to Kerguelen.

Réunion. The bathymetry and geoid of the Réunion hotspot have been studied by Bonneville et al. [1988]. The swell is evident from both data sets. The stagnation distance is about 300 km (Figure 13). The swell height is 1100 m [Crough, 1983]. The cross section is about 900 km^2 . The spreading rate is 28.5 mm yr^{-1} . The buoyancy flux is thus 1.9 Mg s^{-1} . The volume flux from (10) is $85\text{ m}^3\text{ s}^{-1}$. The temperature implied by these numbers is 225°C in agreement with the other hotspots.

Afar. The Afar hotspot is similar to Iceland in that a subaerial plateau exists but complicated by the narrow width of the ocean and the spreading on the East African Rift. The strongly affected length of the Red Sea and Gulf of Aden rifts is about 600 km and the average spreading rate over this interval is about 17 mm yr^{-1} [Joffe and Garfunkel, 1987]. About 400 km of the East African Rift with a spreading rate of 2.5 mm yr^{-1} is strongly affected. Assuming that the flow supplies lithosphere and asthenosphere thicknesses of 100 km, as was done for Iceland, equation (1) yields a volume flux of

$53\text{ m}^3\text{ s}^{-1}$. The buoyancy flux (assuming it takes an average excess of 225°C to make subaerial plateaus) is 1.2 Mg s^{-1} .

Grand Total Global Flux

The buoyancy fluxes estimated for the 37 hotspots discussed above along with a reliability are given in Table 1 along with the flux estimates of Davies [1988a]. The Hawaiian hotspot is clearly the largest. The fluxes determined for hotspots vary by a factor of 20 even considering only plumes with good tracks. Thus one should not extrapolate the Hawaiian flux by multiplying by the global number of hotspots. The total buoyancy flux is 54.9 Mg s^{-1} . Some hotspots, particularly continental ones, are omitted, and the flux of some of the weaker hotspots overestimated. Although the estimates for individual hotspots differ, the total is in excellent agreement with Davies' [1988a] estimate of 41.3 Mg s^{-1} , which omits on-ridge hotspots but includes more continental hotspots within Africa. The difference between the two estimates indicates the true uncertainty. Multiplying by C/α gives an equivalent surface heat flow of 4.48 mW m^{-2} averaged over the planet.

DISCUSSION AND PHENOMENOLOGY

As noted by Davies [1988a], the total heat flux from plumes is compatible with the heat coming from cooling the core. The global heat flow coming from the mantle is about 74 mW m^{-2} [Sleep and Langan, 1981]. About half this heat comes from internal radioactivity and half from cooling [e.g., Christensen, 1985]. About $4/5$ of the heat capacity of Earth is in the mantle and $1/5$ in the core if latent heat is ignored [Stacey, 1980]. Thus, if the core and mantle cool at the same rate, cooling of the core supplies 10% of the heat in comparison to the estimated 6%. More precisely, a heat loss of 4 mW m^{-2} would cool the core at 50°C in 1 b.y. if not balanced by heat sources. (The specific heat for the core given by Stacey [1980] implies that 1 W m^{-2} cools the core 12.84°C in 1 m.y.)

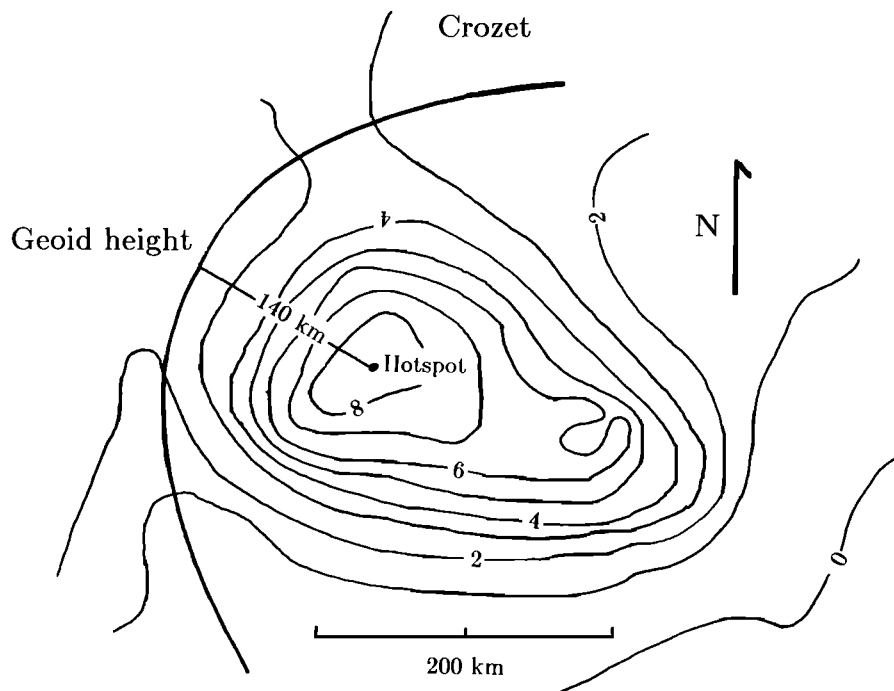


Fig. 12. The geoid height in meters near Crozet is contoured in meters [Courtney and Recq, 1986]. A 140-km stagnation curve is fit by eye to the anomaly. The model hotspot is at the dot.

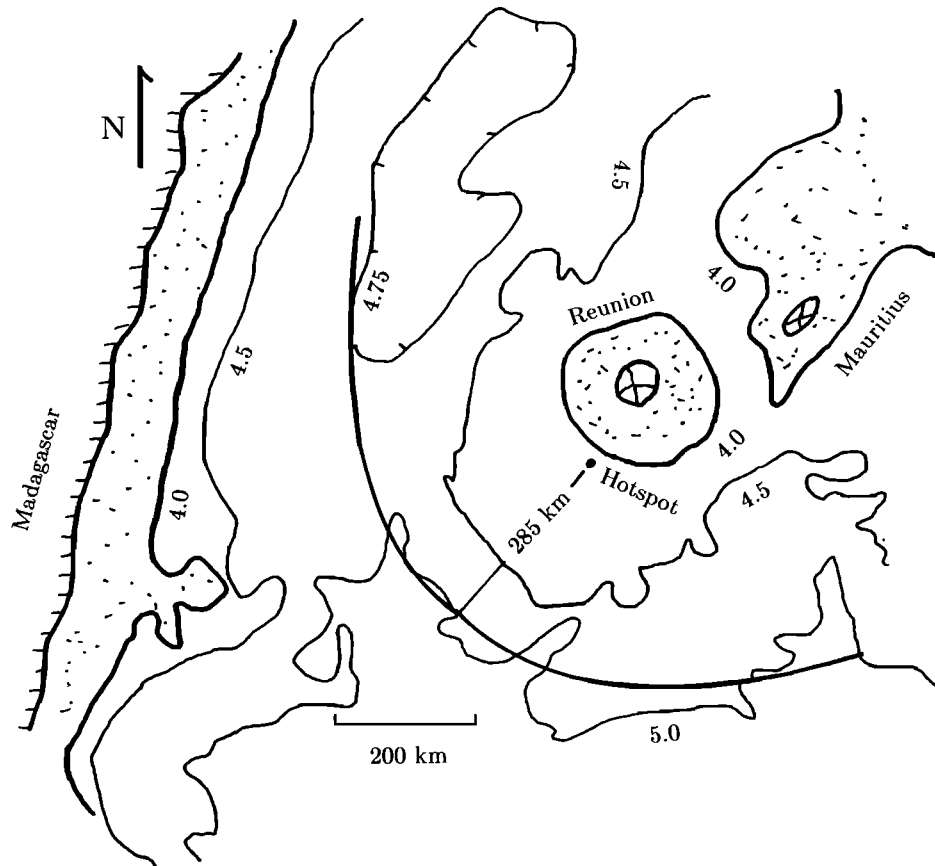


Fig. 13. The ocean depth in meters near Réunion is contoured in kilometers [Bonneville *et al.*, 1988]. The 5-, 4.5-, 4-, and 0-km contours are plotted. The 4.75-km contour is plotted in the basin between Madagascar and Réunion. The interval between 4- and 0-km depth is shaded. A 285-km stagnation curve is fit by eye to the 5-km contour. The model hotspot is indicated by the dot.

Spatial Distribution of Plumes and their Fluxes

It is well established that hotspots are nonrandomly distributed on a global basis [Vogt, 1981; Pollack *et al.*, 1981; Stefanick and Jurdy, 1984; Richards *et al.*, 1988; Weinstein and Olson, 1989]. There are enough plumes and enough variation in plume fluxes to make additional inferences from the distribution. These fluxes provide an instantaneous picture, which could be improved by flux histories for hotspot tracks. Several hotspots, including Bermuda, Louisville, Tristan, Great Meteor, and Caroline, appear to have waned recently. (The older strong track permits location of these hotspots which might otherwise be missed.) Others, including Crozet, may have become stronger.

Hotspots are preferentially located near ridge axes [Weinstein and Olson, 1989]. This is partly the result of a capture mechanism. If the ridge axis is not fixed in the hotspot frame, it may collide with a hotspot. Once the ridge axis is on the hotspot, continual ridge jumps are required to keep there. When the hotspot volume flux is comparable to the material normally supplied to a significant length of ridge, axis jumps occur, as in Iceland [Vink, 1984]. It helps also if the velocity of hotspot perpendicular to the ridge is small as with Juan de Fuca and Galapagos. Conversely, the weaker Atlantic hotspots appear to have crossed the ridge without capturing it. Tristan was an on-ridge hotspot until it waned. The current total buoyancy flux for the on-ridge or near ridge hotspots, Easter, Iceland, Afar, Azores, Galapagos, Tristan, Juan de Fuca, and Bowie is 9.3 Mg s^{-1} similar to Hawaii and less than 1/5 of the global

total. This implies that capture of the ridge by hotspots is inefficient or that large hotspots do not frequently encounter the ridge axis.

The most active hotspots occur only on the rapidly moving plates, while weak hotspots occur on both fast and slow plates. This distribution is partly the result of the effect of plumes on plate boundaries. A strong hotspot on a slowly moving plate weakens the plate and may cause breakup of the plate [Morgan, 1981]. Thus the plate velocity may increase. For example, Réunion is associated with the breakup of India.

Once effect of plumes on ridge location is considered, it can be seen that hotspot tracks are often oblivious to the surface plate geometry. I have already made the argument that ridge crossing is strong evidence that plumes from great depth produce hotspots. An argument against stress and for plumes can be made for other hotspots near plate boundaries. The Samoan hotspot has followed the general Pacific track direction even though it has approached the northern end of the Tonga arc where intraplate stresses should be complicated. A similar argument might be made for the Caroline hotspot, although it has waned to some extent.

Plume families. Some hotspots can be grouped into closely spaced families. Bouvet, Meteor, Discovery, and Tristan are one group that might include Martin and Fernando. Cape Verde, Canary, and Madeira (if it is considered separate) are another. The East Australia and two Tasman sea chains are a third group. Juan de Fuca and Bowie are another if they are in fact associated with plumes. As noted already the Pacific

TABLE 1. Hotspot Buoyancy Flux

Hotspot	Flux,* Mg s ⁻¹	Reliability	Flux,† Mg s ⁻¹
Afar	1.2	good	
Australia, East	0.9	fair	
Azores	1.1	fair	
Baja	0.3	poor	
Bermuda	1.1	good	1.5
Bouvet	0.4	fair	
Bowie	0.3	poor	0.8
Canary	1.0	fair	
Cape Verde	1.6	good	0.5
Caroline	1.6	poor	
Crozet	0.5	good	
Discovery	0.5	poor	0.4
Easter	3.3	fair	
Fernando	0.5	poor	0.9
Galapagos	1.0	fair	
Great Meteor	0.5	poor	0.4
Hawaii	8.7	good	6.2
Hoggar	0.9	fair	0.4
Iceland	1.4	good	
Juan de Fuca	0.3	fair	
Juan Fernandez	1.6	poor	1.7
Kerguelen	0.5	poor	0.2
Louisville	0.9	poor	3.0
Macdonald	3.3	fair	3.9
Marqueses	3.3	fair	4.6
Martin	0.5	poor	0.8
Meteor	0.5	poor	0.4
Pitcairn	3.3	fair	1.7
Réunion	1.9	good	0.9
St. Helena	0.5	poor	0.3
Samoa	1.6	poor	
San Felix	1.6	poor	2.3
Tahiti	3.3	fair	5.8
Tasman, Central	0.9	poor	
Tasman, East	0.9	poor	
Tristan	1.7	fair	0.5
Yellowstone	1.5	fair	
Sum	54.9		

*This paper.

†Davies [1988a].

Superswell has been considered a hot line [Bonatti *et al.*, 1977], extending from Caroline to San Felix and/or Juan Fernandez.

In contrast, some hotspots are isolated. In particular, the strongest hotspot, Hawaii, is isolated with the nearest active hotspots over 2000 km away. Iceland and maybe Réunion belong to this class. These plumes may be at the centers of columnar upwellings. Other hotspots, such as Azores, Bermuda, Crozet, Kerguelen, and St. Helena are neither widely separated from other hotspots nor obvious members of families.

The close spacing of many hotspots has been used as an argument against mantle plumes [e.g., Mchone *et al.*, 1987] because long closely spaced conduits from the core seem unreasonable. Alternatively, some plumes may arise from tabular upwellings of the basal thermal boundary layer in the mantle [Sleep *et al.*, 1988]. The temperature dependence of viscosity should cause the slowly moving parts of the upwelling to cool and become more viscous while the rapidly moving parts remain hot and take up the bulk of the flow. If plume families are real, material may ascend from the basal mantle boundary layer partly as two-dimensional tabular upwellings which break-up into plumes at shallower depths.

The Earth's mantle is believed to have cooled 200°C to 300°C over the last 3 b.y. [Christensen, 1985]. The difference

between this mantle cooling rate and core cooling rate of 50°C b.y.⁻¹ inferred from the global heat flux from hotspots implies that the temperature contrast just above the core-mantle boundary has increased with time. The viscosity contrast between the upwelling material and the surrounding mantle which permits the rapid ascent of plumes thus has also increased with time. Sleep *et al.* [1988] used this reasoning to show that plumes may be a geologically recent occurrence on Earth. They noted that plumes might first originate in families at the expense of two-dimensional tabular upwellings. They used the occurrence of plume families as support of this hypothesis. Recognition of the 1267 Ma MacKenzie igneous events as the effects of a plume head [LeCheminant and Heaman, 1989] pushes the initiation of vigorous plumes back to that time.

New hotspots. Plumes penetrating pristine mantle are mushroom-shaped with a large head and a thin stem [Whitehead and Luther, 1975; Olson and Singer, 1985]. Isolated plumes which penetrate pristine mantle might be expected to have larger heads than family plumes which grow at the expense of an already hot upwelling. There is some information to support this inference. The Deccan traps and the Réunion hotspot track, the most obvious example of a new hotspot [Courtilot *et al.*, 1986; Richards *et al.*, 1989], is more or less isolated. Other examples of isolated features, include the Ontong-Java plateau and the Louisville track. The Crozet, here associated with the Karroo basalts [Richards *et al.*, 1989], is also isolated. Parana basalts are, however, associated with the Tristan track, which is the dominant member of the family of South Atlantic hotspots. The Columbia basalts and Yellowstone track are isolated only if Juan de Fuca, Bowie, and Raton are not associated with their own plumes.

The area strongly affected by modern plume heads is typically 1000 km in radius (data from White and McKenzie [1989]). Such regions are observed from Greenland (Iceland plume), Parana (Tristan plume), Deccan (Réunion plume), Afar, and Karroo (Crozet plume). In contrast, much more modest areas of excess volcanism are associated with families of plateaus on the coasts of western Australia and the eastern United States (data from White and McKenzie [1989]). No attempt is made here to estimate the volume of plume heads. This task is somewhat difficult because the ratio of plume material to melt varies by a factor of 10 between Hawaii and Iceland. The extent of flood basalts is partly controlled by dikes which radiate from the hotspot, rather than underlying melting. For example, such dikes radiate 2400 km from the center of the 1267 Ma MacKenzie swarm [LeCheminant and Heaman, 1989].

Only a small fraction of the hotspots are associated with postulated heads. Either a significant fraction of plumes formed without large heads, or plumes last long enough that older heads cannot be found and matched with plumes. The presence of long-lived tracks, such as Great Meteor-Monteregian Hills, is support for the latter. So does the recognition of the 1267 Ma MacKenzie igneous event as a plume head [LeCheminant and Heaman, 1989]. I do note that the new plumes discussed above all (except Crozet where the early flux is unknown) had buoyancy fluxes over 1.4 Mg s⁻¹ soon after they became active.

Fate of Heat Supplied by Plumes

Plume material is supplied initially to the asthenosphere and then the heat is transferred to the lower lithosphere. Some of this heat eventually reaches the surface as excess heat flow, while the rest of the heat is subducted with the lithosphere [Davies, 1988a]. An estimate of this division is needed if one

wishes to include plumes in a parameterized convection model. Statistical estimates are obtained by considering plumes a random phenomenon. Direct estimates are obtained using currently subducting swells or extrapolating crust near active hotspots to trenches.

Statistical estimate. Hotspots may be treated as a statistical feature on the oceanic crust. The approach is practical because hotspots seem independent of the details of plate geometry and the probability that ocean crust gets subducted is relatively independent of its age [Sclater *et al.*, 1980]. First, hotspot swells are generally wider than the depth at which heat is implaced. Horizontal conduction is thus ignored, and the heat source is considered an infinite horizontal plane within a half-space. The excess temperature from a heat source which liberates $Q\rho c$ heat per area at depth z_0 is [Carlaw and Jaeger, 1959, p. 259]

$$\Delta T = \frac{Q}{2} (\pi\kappa t)^{-1/2} \cdot \left\{ \exp \left[\frac{-(z - z_0)^2}{4\kappa t} \right] - \exp \left[\frac{-(z + z_0)^2}{4\kappa t} \right] \right\} \quad (35)$$

where z is depth, κ is thermal diffusivity, and t is time since the heat source appeared. The excess heat flow is

$$q = k \left[\frac{\partial T}{\partial z} \right]_{z=0} = 4z_0 k Q \pi^{-1/2} (4\kappa t)^{-3/2} \exp \left[\frac{-z_0^2}{4\kappa t} \right] \quad (36)$$

These equations are intended to be valid after the lithosphere has moved away from the hotspot and convection has transferred the excess heat to the lower lithosphere. They do not represent the actual heating in detail.

If no subduction occurred, the total heat flux would eventually be that supplied by the heat source

$$Q\rho c = \int_0^{\infty} q \, dt \quad (37)$$

Assuming that the probability of subduction is independent of both plate age and hotspot age requires weighting the heat flow by the probability (an exponential of time) that the crust still exists (has not been subducted) at time t after the hotspot occurred. The heat which actually reaches the surface is then

$$\int_0^{\infty} q \exp(-t/t_s) dt = (Q\rho c) \exp[-2z_0/(4\kappa t_s)^{1/2}] \quad (38)$$

where t_s is the time constant for subduction. The fraction of heat that escapes, rather than being subducted, is the exponential term.

The depth of emplacement of the heat source z_0 is related to the plate thickness and hence the plate age at the time of the hotspot. That is, excess heat is supplied to near the base of the previous thermal lithosphere [e.g., Cazenave *et al.*, 1988]. Here, this depth is crudely estimated as the scale thickness of the lithosphere $\sqrt{4\kappa t_p}$, where t_p is plate age. At that depth, the lithosphere has cooled to 84% of its original temperature.

The global fraction of heat which escapes is obtained by assuming that heat introduced by plumes on the average is independent of plate age. The escaping fraction then needs to be weighted by the amount of plate of each age at the time of the hotspot

$$F = t_s^{-1} \int_0^{\infty} \exp[-2t_p^{1/2}/t_s^{1/2}] \exp[-t_p/t_s] dt_p \\ = 1 - e \pi^{1/2} \operatorname{erfc}(1) = 0.24 \quad (39)$$

where t_p is the dummy variable for plate age and t_s is the subduction time constant for both normal lithosphere and hotspot lithosphere. This result is independent of the average life of oceanic crust.

Some direct inferences. As noted earlier, plumes are not randomly distributed on Earth. If plumes in fact originate at the base of the mantle, they should avoid cool regions where many slabs have penetrated [Chase and Sprowl, 1983]. There thus should be some tendency for hotspot swells to form away from subduction zones and to get subducted later than typical crust. To some extent this is true. The swells of the Atlantic and Indian hotspots are mostly between passive margins and ridges and cannot be subducted without a major plate reorganization. The Emperor swell is being subducted at the farthest possible point away from Hawaii. Only Samoa, San Felix, Juan Fernandez, Bowie, and Juan de Fuca are near active subduction zones.

The swells thus are subducted less frequently than ordinary oceanic crust. I model this effect by assuming that swells take proportionally longer to subduct on the average than ordinary oceanic crust. Then equation (38) becomes

$$\int_0^{\infty} q \exp(-t/t_{sw}) dt = (Q\rho c) \exp[-2z_0/(4\kappa t_{sw})^{1/2}] \quad (40)$$

where t_{sw} is the subduction time constant for swells. This subduction time and the time constant t_s which governs the distribution of the plate age of the lithosphere reactivated by hotspots need to be distinguished in (39)

$$F = t_s^{-1} \int_0^{\infty} \exp[-2t_p^{1/2}/t_s^{1/2}] \exp[-t_p/t_s] dt_p \\ = 1 - (t_s/t_{sw})^{1/2} \exp(t_s/t_{sw}) \pi^{1/2} \operatorname{erfc}(t_s^{1/2}/t_{sw}^{1/2}) \quad (41)$$

[Gradshteyn and Ryzhik, 1965, integral 3.462,5]. If swells take twice as long to subduct as normal crust, $t_{sw} \approx 2t_s$, the fraction of heat which escapes is 34%.

Some correction is also needed for plumes on continents where all the heat can eventually escape. However, larger plumes break continental plates and thus erupt on continents only briefly. The present continental plumes are likely to have fluxes between that of Yellowstone and those of the weaker Atlantic hotspots. Thus about 10% of the heat and buoyancy flux of global hotspots may be associated with continental ones. That is, between 1/4 and 1/3 of the 90% of the heat associated with oceanic hotspots and all of the 10% of the heat on continents escape. This implies that globally 33-40% of the heat supplied by plumes escapes before it is subducted. In their parameterized convection calculations, Sleep *et al.* [1988] assumed that all the heat lost by the core became mixed into the mantle rather than escaping at the surface. From the above analysis this assumption should not lead to gross errors, although improved calculations could be made taking this effect into account.

CONCLUSIONS

The hypothesis that mantle plumes ascend from the base of the mantle was originally proposed to explain the track direc-

tions of hotspots. This hypothesis provides an explanation of several additional features. In particular, plumes supply material which spreads out horizontally beneath the lithosphere. Heat is then transferred from the abnormally hot asthenospheric material to the lithosphere by convection and conduction. The excess heat and buoyancy of swells downstream from hotspots move with the lithospheric plate. The shape of the snout of swells is attributed to stagnation streamlines which separate material supplied by the plumes from ambient asthenosphere.

Hot asthenosphere near the plume may be detected by geoid and elevation anomalies. The geometry for doing this is best on slowly moving plates. Unfortunately, the effects of long-wavelength geoid anomalies, volcanic edifices, and flexure need to be filtered from the model and the data in a consistent manner. Observations are consistent with an average excess temperature around 200°C in the asthenosphere. Although the error bounds on this temperature are great, an excess of 1000°C is not compatible with the observations. This poses a difficulty in having the core much hotter than the overlying mantle because the temperature contrast in vigorous plumes is expected to scale to the temperature contrast in across the basal boundary layer [Davies, 1988a].

The flux of on-ridge hotspots such as Iceland, Azores, and Afar is similar to that of off-ridge hotspots. The excess temperature obtained from petrological studies of Icelandic and Hawaiian lavas are similar, around 200°C. Again the error bounds on the temperature are large, particularly because the origin of mid-oceanic ridge basalts is not well understood. Thus on-ridge and off-ridge hotspots may be the effect of similar plumes. This inference is further supported as hotspots appear to have crossed ridge axes or in the case of Tristan recently evolved to being off-axis.

The global excess heat flux at hotspots is 4 mW m⁻² in agreement with the compilation of Davies [1988a]. As noted by Davies, this is what is expected to be emerging from the core. Much of the heat is later subducted back into the mantle.

Finally, how can one refine the estimates of plume flux and the dynamic processes associated with swells? A major limitation in studying swells is that uplift and subsidence rates are inferred from excess elevation as a function of distance along the swell. Uplift or subsidence have been determined directly only in a few studies and these have not had detailed time resolution. The swells of weak hotspots might be resolved from uplift and subsidence data but are not evident on excess elevation maps. In principle, atolls and guyots are needed to determine the subsidence of the axis of swells. Uplift and subsidence might also be inferred from onlap relationships of turbidity plains and the passage of older seamounts through the carbonate compensation depth. This is clearly a major undertaking.

Acknowledgments. The research was supported in part by the National Science Foundation grants EAR85-18459 and EAR87-19278. Discussions with Beth Robinson, Mark Richards, Brad Hager, Mark Anders, W. Jason Morgan, Richard Gordon, Donna Jurdy, Jean-Guy Schilling, Geoff Davies, Marcia McNutt, Dave Clague, Tony LeCheminant, Uri ten Brink, and Clem Chase were helpful at various times. I also thank the staff of the geology library at Stanford for help in locating references.

REFERENCES

- Allan, J. F., B. L. Cousens, R. L. Chase, M. P. Gorton, and P. J. Michael, Alkaline lavas from the Tuzo Wilson seamounts, NE Pacific: Volcanism at a complex ridge-transform intersection (abstract), *Eos Trans. AGU*, 69, 1503, 1988.
- Anders, M. H., J. W. Geissman, L. A. Piety, and J. T. Sullivan, Parabolic distribution of circum-eastern Snake River Plain seismicity and latest Quaternary faulting: Migratory pattern and association with Yellowstone hotspot, *J. Geophys. Res.*, 94, 1589-1621, 1989.
- Barker, P. F., Tectonic evolution and subsidence history of the Rio Grande Rise, *Initial Rep. Deep Sea Drill. Proj.*, 72, 953-976, 1983.
- Bédard, J. H., The opening of the Atlantic, the Mesozoic New England igneous province, and mechanisms of continental break-up, *Tectonophysics*, 113, 209-232, 1985.
- Black, R., L. Lameyre, and B. Bonin, The structural setting of alkaline complexes, *J. Afr. Earth Sci.*, 3, 5-16, 1985.
- Bonatti, E., C. G. A. Harrison, D. E. Fisher, J. Honnorez, J. G. Schilling, J. J. Stipp, and M. Zentelli, Easter volcanic chain (southeast Pacific): A mantle hot line, *J. Geophys. Res.*, 82, 2457-2478, 1977.
- Bonneville, A., J. P. Barriot, and R. Bayer, Evidence from geoid data of a hotspot origin for the southern Mascarene Plateau and Mascarene Islands (Indian Ocean), *J. Geophys. Res.*, 93, 4199-4212, 1988.
- Bowin, C., G. Thompson, and J. G. Schilling, Residual geoid anomalies in the Atlantic Ocean basin: Relationship to mantle plumes, *J. Geophys. Res.*, 89, 9905-9918, 1984.
- Brodholt, J. P., and R. Batiza, Global systematics of unaveraged mid-ocean ridge basalt compositions: Comment on "Global correlations of ocean ridge basalt chemistry with axial depth and crust thickness" by E. M. Klein and C. H. Langmuir, *J. Geophys. Res.*, 94, 4231-4239, 1989.
- Brott, C. A., D. D. Blackwell, and J. P. Ziagos, Thermal and tectonic implications of heat flow in the eastern Snake River Plain, Idaho, *J. Geophys. Res.*, 86, 11,709-11,734, 1981.
- Carlsaw, H. S., and J. C. Jaeger, *Conduction of Heat in Solids*, 510 pp., Clarendon, Oxford, 1959.
- Castillo, P., R. Batiza, D. Vanko, E. Malavassi, J. Barquero, and E. Fernandez, Anomalous young volcanoes on old hot-spot traces, I, Geology and petrology of Cocos Island, *Geol. Soc. Am. Bull.*, 100, 1400-1414, 1988.
- Cazenave, A., K. Dominh, M. Rabinowicz, and G. Ceuleneer, Geoid and depth anomalies over ocean swells and troughs: Evidence of an increasing trend of the geoid to depth ratio with age of plate, *J. Geophys. Res.*, 93, 8064-8077, 1988.
- Chase, C. G., and D. R. Sprowl, The modern geoid and ancient plate boundaries, *Earth Planet. Sci. Lett.*, 62, 314-320, 1983.
- Christensen, U., Thermal models for the Earth, *J. Geophys. Res.*, 90, 2995-3008, 1985.
- Clague, D. A., and G. B. Dalryple, The Hawaiian-Emperor volcanic chain, part 1, Geologic evolution, Volcanism in Hawaii, *U.S. Geol. Surv. Prof. Pap.*, 1350, 5-54, 1987.
- Courtillot, V., J. Besse, D. Vandamme, R. Montigny, J.J. Jaeger, and H. Cappetta, Deccan flood basalts at the Cretaceous/Tertiary boundary?, *Earth Planet. Sci. Lett.*, 80, 361-374, 1986.
- Courtney, R. C., and M. Recq, Anomalous heat flow near the Crozet Plateau and mantle convection, *Earth Planet. Sci. Lett.*, 79, 373-384, 1986.
- Courtney, R. C., and R. S. White, Anomalous heat flow and geoid across the Cape Verde Rise: Evidence for dynamic support from a thermal plume in the mantle, *Geophys. J. R. Astron. Soc.*, 87, 815-868, 1986.
- Craig, C. H., and D. McKenzie, The existence of a thin low-viscosity layer beneath the lithosphere, *Earth Planet. Sci. Lett.*, 78, 420-426, 1986.
- Crough, S. T., Thermal origin of hot-spot swells, *Geophys. J. R. Astron. Soc.*, 55, 451-469, 1978.
- Crough, S. T., Free-air gravity over the Hoggar Massif, northwestern Africa: Evidence for alteration of the lithosphere, *Tectonophysics*, 77, 189-202, 1981.
- Crough, S. T., Hotspot swells, *Annu. Rev. Earth Planet. Sci.*, 11, 163-193, 1983.
- Dalryple, G. B., D. A. Clague, T. L. Vallier, and H. M. Menard, ⁴⁰Ar/³⁹Ar age, petrology, and tectonic significance of some seamounts in the Gulf of Alaska, in *Seamounts, Islands, and Atolls*, Geophys. Monogr. Ser., vol. 43, edited by B. Keating and R. Batiza, pp. 297-315, AGU, Washington, D.C., 1987.
- Davies, G. F., Ocean bathymetry and mantle convection, 1, Large-scale flow and hotspots, *J. Geophys. Res.*, 93, 10,467-10,480, 1988a.
- Davies, G. F., Ocean bathymetry and mantle convection, 2, Small-scale flow, *J. Geophys. Res.*, 93, 10,481-10,488, 1988b.
- Detrick, R. S., and S. T. Crough, Island subsidence, hotspots and lithospheric thinning, *J. Geophys. Res.*, 83, 1236-1244, 1978.
- Detrick, R. S., R. P. von Herzen, B. Parsons, D. Sandwell, and M. Dougherty, Heat flow observations on the Bermuda Rise and thermal models of mid-plate swells, *J. Geophys. Res.*, 91, 3701-3723, 1986.
- Duncan, R. A., Age progressive volcanism in the New England

- seamounts and the opening of the central Atlantic Ocean, *J. Geophys. Res.*, **89**, 9980-9990, 1984.
- Duncan, R. A., and D. A. Clague, Pacific plate motion recorded by linear volcanic chains, in *The Ocean Basins and Margins*, vol. 7A, *The Pacific Ocean*, edited by A. E. M. Nairn, F. G. Stehi, and S. Uyeda, pp. 89-121, Plenum, New York, 1985.
- Eaby, J., D. A. Clague, and J. R. Delaney, Sr isotopic variations along the Juan de Fuca ridge, *J. Geophys. Res.*, **89**, 7883-7890, 1984.
- Elithon, D., J. F. Casey, and S. Komar, Mineral chemistry of ultramafic cumulates from the North Arm Mountain Massif of the Bay of Islands Ophiolite: Implication for high pressure fractionation of oceanic basalts, *J. Geophys. Res.*, **87**, 8717-8734, 1982.
- Giret, A., and J. Lameyre, Inverted alkaline-tholeiitic sequences related to lithospheric thickness in the evolution of continental rifts and oceanic islands, *J. Afr. Earth Sci.*, **3**, 261-268, 1985.
- Gordon, R. G., and D. M. Jurdy, Cenozoic global plate motions, *J. Geophys. Res.*, **91**, 12,389-12,406, 1986.
- Goslin, J., and M. Diament, Mechanical and thermal isostatic response of the Del Cano Rise and the Crozet Bank (southern Indian Ocean) from altimetry data, *Earth Planet. Sci. Lett.*, **84**, 285-294, 1987.
- Gradshteyn, I. S., and I. M. Ryzhik, *Table of Integrals, Series, and Products*, Translated from Russian by A. Jeffery, 1086 pp., Academic, San Diego, Calif., 1965.
- Grimison, N. L., and W.-P. Chen, Earthquakes in the Davie Ridge-Madagascar region and the southern Nubian-Somalian plate boundary, *J. Geophys. Res.*, **93**, 10,439-10,450, 1988.
- Hayes, D. E., Age-depth relationships and depth anomalies in the southeast Indian Ocean and South Atlantic Ocean, *J. Geophys. Res.*, **83**, 2937-2954, 1988.
- Hey, R., Tectonic evolution of the Cocos-Nazca spreading center, *Geol. Soc. Am. Bull.*, **88**, 1404-1420, 1977.
- Hey, R., G. L. Johnson, and A. Lowrie, Recent plate motions in the Galapagos area, *Geol. Soc. Am. Bull.*, **88**, 1385-1403, 1977.
- Joffe, S., and Z. Garfunkel, Plate kinematics of the circum Red Sea—A re-evaluation, *Tectonophysics*, **141**, 5-22, 1987.
- Jung, W.-Y., and P. D. Rabinowitz, Residual geoid anomalies of the North Atlantic Ocean and their tectonic implications, *J. Geophys. Res.*, **91**, 10,383-10,397, 1986.
- Karsten, J. L., and J. R. Delaney, Hot spot—ridge crest convergence in the northeast Pacific, *J. Geophys. Res.*, **94**, 700-712, 1989.
- Keating, B. H., D. P. Matthey, C. E. Helsley, J. J. Naughton, and D. Epp, Evidence for a hotspot origin of the Caroline Islands, *J. Geophys. Res.*, **89**, 9937-9948, 1984.
- Klein, E. M., and C. H. Langmuir, Global correlations of ocean ridge chemistry with axial depth and crust thickness, *J. Geophys. Res.*, **92**, 8089-8115, 1987.
- Klein, E. M., and C. H. Langmuir, Local versus global variations in ocean ridge basalt composition: A reply, *J. Geophys. Res.*, **94**, 4241-4252, 1989.
- Lawver, L. A., J. G. Sclater, and L. Meinke, Mesozoic and Cenozoic reconstructions of the South Atlantic, *Tectonophysics*, **114**, 233-254, 1985.
- LeCheminant, A. N., and L. M. Heaman, MacKenzie igneous events, Canada: Middle Proterozoic hotspot magmatism associated with ocean opening, *Earth Planet. Sci. Lett.*, **96**, 38-48, 1989.
- Lipman, P. W., D. A. Clague, J. G. Moore, and R. T. Holcomb, South Arch volcanic field—Newly identified young lava flows on the seafloor south of the Hawaiian ridge *Geology*, **17**, 611-614, 1989.
- Lonsdale, P., Geography and history of the Louisville hotspot chain in the southwest Pacific, *J. Geophys. Res.*, **93**, 3078-3104, 1988.
- Mammerickx, J., Depth anomalies in the Pacific: Active, fossil, and precursor, *Earth Planet. Sci. Lett.*, **53**, 147-157, 1981.
- Mammerickx, J., D. F. Naar, and R. L. Tyce, The Mathematician paleoplate, *J. Geophys. Res.*, **93**, 3025-3040, 1988.
- McDougall, I., and R. A. Duncan, Age progressive volcanism in the Tasman seamounts, *Earth Planet. Sci. Lett.*, **89**, 207-220, 1988.
- McHone, J. G., and J. R. Butler, Mesozoic igneous provinces of New England and the opening of the North Atlantic Ocean, *Geol. Soc. Am. Bull.*, **95**, 757-765, 1984.
- McHone, J. G., M. E. Ross, and J. D. Greenough, Mesozoic dyke swarms of eastern North America, Mafic Dyke Swarms, Spec. Pap. Geol. Assoc. Can., **34**, edited by H. C. Halls and W. F. Fahrig, 243-256, 1987.
- McKenzie, D. P., The generation and compaction of partial molten rock, *J. Petrol.*, **25**, 713-765, 1984.
- McNutt, M. K., Lithospheric flexure and thermal anomalies, *J. Geophys. Res.*, **89**, 11,180-11,194, 1984.
- McNutt, M., Temperature beneath mid-plate swells: The inverse problem, in *Seamounts, Islands, and Atolls*, *Geophys. Monogr. Ser.*, vol. 43, edited by B. Keating and R. Batiza, pp. 123-132, AGU, Washington, D.C., 1987.
- McNutt, M., Thermal and mechanical properties of the Cape Verde Rise, *J. Geophys. Res.*, **93**, 2784-2794, 1988.
- McNutt, M., and K. Fischer, The South Pacific superswell, in *Seamounts, Islands, and Atolls*, *Geophys. Monogr. Ser.*, vol. 43, edited by B. Keating and R. Batiza, pp. 25-34, AGU, Washington, D.C., 1987.
- McNutt, M., and L. Shure, Estimating the compensation depth of the Hawaiian swell with linear filters, *J. Geophys. Res.*, **91**, 13,915-13,924, 1986.
- Minster, J. B., and T. H. Jordan, Present-day plate motions, *J. Geophys. Res.*, **83**, 5331-5354, 1978.
- Morgan, W. J., Rodriguez, Darwin, Amsterdam, ..., A second type of hotspot island, *J. Geophys. Res.*, **83**, 5355-5360, 1978.
- Morgan, W. J., Hotspot tracks and the opening of the Atlantic and Indian oceans, in *The Sea*, vol. 7, *The Oceanic Lithosphere*, edited by C. Emiliani, pp. 443-487, John Wiley, New York, 1981.
- Morse, P. M., and H. Feshbach, *Methods of Theoretical Physics*, 2 vols., 1978 pp., McGraw-Hill, New York, 1953.
- Mutter, J. C., W. R. Buck, and C. M. Zehnder, Convective partial melting, 1. A model for the formation of thick basaltic sequences during the initiation of spreading, *J. Geophys. Res.*, **93**, 1031-1048, 1988.
- Olson, P., and H. Singer, Creeping plumes, *J. Fluid. Mech.*, **158**, 511-531, 1985.
- Pollack, H. N., I. G. Gass, R. S. Thorpe, and D. S. Chapman, On the vulnerability of lithospheric plates to midplate volcanism: Reply to comments by P. R. Vogt, *J. Geophys. Res.*, **86**, 961-966, 1981.
- Presnall, D. C., and J. D. Hoover, Composition and depth of origin of primary mid-ocean ridge basalts, *Contrib. Mineral. Petrol.*, **87**, 170-178, 1984.
- Renkin, M. L., and J. G. Sclater, Depth and age in the North Pacific, *J. Geophys. Res.*, **93**, 2919-2936, 1988.
- Richards, M. A., R. A. Duncan, and V. E. Courtillot, Flood basalts and hotspot tracks: Plume heads and tails *Science*, **246**, 103-107, 1989.
- Richards, M. A., B. H. Hager, and N. H. Sleep, Dynamically supported geoid highs over hotspots: Observation and theory, *J. Geophys. Res.*, **93**, 7690-7708, 1988.
- Robinson, E. M., The topographic and gravitational expression of density anomalies due to melt extraction in the uppermost oceanic mantle, *Earth Planet. Sci. Lett.*, **90**, 221-228, 1988.
- Robinson, E. M., and B. Parsons, Effect of a shallow low-velocity zone on small-scale instabilities under cooling oceanic plates, *J. Geophys. Res.*, **93**, 3469-3479, 1988.
- Robinson, E. M., B. Parsons, and S. F. Daly, The effect of a shallow low viscosity zone on the apparent compensation of mid-plate swells, *Earth Planet. Sci. Lett.*, **82**, 335-348, 1987.
- Robinson, E. M., B. Parsons, and M. Driscoll, The effect of a shallow low-viscosity zone on the mantle flow, the geoid anomalies, and the geoid and depth-age relationships at fracture zones, *Geophys. J.*, **93**, 25-43, 1988.
- Saemundsson, K., Subaerial volcanism in the western North Atlantic, in *The Geology of North America*, vol. M, *The Western North Atlantic Region*, edited by P. R. Vogt and B. E. Tucholke, pp. 69-86, Geology Society America, Boulder, Colo., 1986.
- Sandwell, D. T., and K. R. MacKenzie, Geoid height versus topography for oceanic plateaus and swells, *J. Geophys. Res.*, **94**, 7403-7418, 1989.
- Sandwell, D. T., and M. L. Renkin, Compensation of swells and plateaus in the North Pacific: No direct evidence for mantle convection, *J. Geophys. Res.*, **93**, 2775-2783, 1988.
- Schilling, J.G., Iceland mantle plume, geochemical evidence along Reykjanes Ridge, *Nature*, **242**, 565-571, 1973.
- Schilling, J.-G., Geochemical and isotopic variation along the Mid-Atlantic Ridge axis from 79°N to 0°N, in *The Geology of North America*, vol. M, *The Western North Atlantic Region*, edited by P. R. Vogt and B. E. Tucholke, pp. 69-86, Geology Society America, Boulder, Colo., 1986.
- Schlanger, S. O., J. F. Campbell, and M. W. Jackson, Post-Eocene subsidence of the Marshall Islands recorded by drowned atolls on Harrie and Sylvania Guyots, in *Seamounts, Islands, and Atolls*, *Geophys. Monogr. Ser.*, vol. 43, edited by B. Keating and R. Batiza, pp. 165-174, AGU, Washington, D.C., 1987.
- Schroeder, W., The empirical age-depth relation and depth anomalies in the Pacific Ocean basin, *J. Geophys. Res.*, **89**, 9873-9884, 1984.
- Sclater J. G., C. Bowin, R. Hey, H. Hoskins, J. Peirce, J. Phillips, and C. Tapscott, The Bouvet triple junction, *J. Geophys. Res.*, **81**, 1857-1869, 1976.

- Sclater, J. G., C. Jaupart, and D. Galson, The heat flow through the oceanic and continental crust and the heat loss of the earth, *Rev. Geophys.*, **18**, 269-312, 1980.
- Sleep, N. H., Tapping of magmas from ubiquitous mantle heterogeneities: An alternative to mantle plumes?, *J. Geophys. Res.*, **89**, 9980-9990, 1984.
- Sleep, N. H., Lithospheric heating by mantle plumes, *Geophys. J. R. Astron. Soc.*, **91**, 1-12, 1987a.
- Sleep, N. H., An analytic model for a mantle plume fed by a boundary layer, *Geophys. J. R. Astron. Soc.*, **90**, 119-128, 1987b.
- Sleep, N. H., and R. T. Langan, Thermal evolution of the earth: Some recent developments, *Adv. Geophys.*, **23**, 1-23, 1981.
- Sleep, N. H., and B. F. Windley, Archean plate tectonics: Constraints and inferences, *J. Geol.*, **90**, 1129-1234, 1982.
- Sleep, N. H., M. A. Richards, and B. H. Hager, Onset of mantle plumes in the presence of preexisting convection, *J. Geophys. Res.*, **93**, 7672-7689, 1988.
- Stacey, F. D., The cooling Earth: A reappraisal, *Phys. Earth Planet. Inter.*, **22**, 89-96, 1980.
- Stefanick, M., and D. M. Jurdy, The distribution of hotspots, *J. Geophys. Res.*, **89**, 9919-9926, 1984.
- Stillman, C. J., A Canary Island dyke swarm: Implications for the formation of oceanic islands by extensional volcanism, Mafic Dyke Swarms, *Spec. Pap. Geol. Assoc. Can.*, **34**, edited by H. C. Halls and W. F. Fahrig, 243-256, 1987.
- Stolper, E., A phase diagram for mid-ocean ridge basalts: Preliminary results and implications, *Contrib. Mineral. Petrol.*, **74**, 13-28, 1980.
- Storey, M., A. D. Saunders, J. Tarney, I. L. Gibson, M. J. Norry, M. F. Thirlwall, P. Leat, R. N. Thompson, and M. A. Menzies, Contamination of Indian Ocean asthenosphere by the Kerguelen-H Heard mantle plume, *Nature*, **338**, 574-596, 1989.
- Sykes, L. R., Intraplate seismicity reactivation, reactivation of pre-existing zones of weakness, alkaline magmatism and other tectonism post-dating continental fragmentation, *Rev. Geophys.*, **16**, 621-688, 1978.
- Turcotte, D. L., and G. Schubert, *Geodynamics: Applications of Continuum Physics to Geological Problems*, 450 pp., John Wiley, New York, 1982.
- Viereck, L. G., M. F. J. Flower, J. Hertogen, H.-U. Schmincke, and G. A. Jenner, The genesis and significance of N-MORB sub-types, *Contrib. Mineral. Petrol.*, **102**, 112-126, 1989.
- Vink, G. E., A hotspot model for Iceland and the Voring Plateau, *J. Geophys. Res.*, **89**, 9949-9959, 1984.
- Vogt, P. R., On the applicability of thermal conduction models to mid-plate volcanism: Comments on a paper by Gass et al., *J. Geophys. Res.*, **86**, 950-960, 1981.
- Vogt, P. R., B. Zondek, P. W. Fell, N. Z. Cherkis, and R. K. Perry, Seasat altimetry, the North Atlantic geoid, and evaluation of shipborne subsatellite profiles, *J. Geophys. Res.*, **89**, 9885-9904, 1984.
- Von Herzen, R. P., Detrick, R. S., Crough, S. T., D. Epp, and U. Fehn, Thermal origin of the Hawaiian swell: Heat flow evidence and thermal models, *J. Geophys. Res.*, **87**, 6711-6723, 1982.
- Von Herzen, R. P., M. J. Cordery, C. Fang, R. S. Detrick, and C. Fang, Heat flow and the thermal origin of hot spot swells: The Hawaiian swell revisited, *J. Geophys. Res.*, **94**, 13,783-13,800, 1989.
- Wallin, B. H., The northern Hawaiian deep and arch: Interpretation of geologic history from reflection profiling and echo mapping, M.S. thesis, 133 pp., Univ. of Hawaii, Honolulu, 1982.
- Watts, A. B., and U. S. ten Brink, Crustal structure, flexure, and subsidence history of the Hawaiian Islands, *J. Geophys. Res.*, **94**, 10,473-10,500, 1989.
- Watts, A. B., J. K. Weissel, R. A. Duncan, and R. L. Larson, Origin of the Louisville ridge and its relationship to the Eltanin fracture zone system, *J. Geophys. Res.*, **93**, 3051-3077, 1988.
- Weinstein, S. A., and P. L. Olson, The proximity of hotspots to convergent and divergent plate boundaries, *Geophys. Res. Lett.*, **16**, 433-436, 1989.
- White, R., and D. McKenzie, Magmatism at rift zones: The generation of volcanic continental margins and flood basalts, *J. Geophys. Res.*, **94**, 7685-7729, 1989.
- Whitehead, J. A., and D. S. Luther, Dynamics of laboratory diapir and plume models, *J. Geophys. Res.*, **80**, 705-717, 1975.
- Wright, E., and W. M. White, The origin of Samoa: New evidence from Sr, Nd and Pb isotopes, *Earth Planet. Sci. Lett.*, **81**, 151-162, 1987.
- Wyllie, P. J., Solidus curves, mantle plumes, and magma generation beneath Hawaii, *J. Geophys. Res.*, **93**, 4171-4181, 1988.

N. H. Sleep, Department of Geophysics, Stanford University, Stanford, CA 94305.

(Received January 20, 1989;
revised November 9, 1989;
accepted November 14, 1989.)